8-21-2015

Atomic Structure of GRK5 Reveals Distinct Structural Features Novel for G Protein-coupled Receptor Kinases

Konstantin E. Komolov
Thomas Jefferson University

Anshul Bhardwaj
Thomas Jefferson University

Jeffrey L. Benovic
Thomas Jefferson University

THE JOURNAL OF BIOLOGICAL CHEMISTRY VOL. 290, NO. 34, pp. 20629–20647, August 21, 2015

Atomic Structure of GRK5 Reveals Distinct Structural Features Novel for G Protein-coupled Receptor Kinases*◆

Received for publication, February 21, 2015, and in revised form, May 28, 2015 Published, JBC Papers in Press, June 1, 2015, DOI 10.1074/jbc.M115.647297

Konstantin E. Komolov, Anshul Bhardwaj[1], and Jeffrey L. Benovic[2]

From the Department of Biochemistry and Molecular Biology, Thomas Jefferson University, Philadelphia, Pennsylvania 19107

Background: GRK5 is implicated in several human pathologies, but relatively little is known about its structure and function.
Results: High resolution crystal structures of human GRK5 with AMP-PNP and sangivamycin were determined.
Conclusion: GRK5 is found in a partially closed state with its kinase domain C-tail forming novel interactions with nucleotide and the N-lobe.
Significance: The GRK5 structure provides important insight into its function.

G protein-coupled receptor kinases (GRKs) are members of the protein kinase A, G, and C families (AGC) and play a central role in mediating G protein-coupled receptor phosphorylation and desensitization. One member of the family, GRK5, has been implicated in several human pathologies, including heart failure, hypertension, cancer, diabetes, and Alzheimer disease. To gain mechanistic insight into GRK5 function, we determined a crystal structure of full-length human GRK5 at 1.8 Å resolution. GRK5 in complex with the ATP analog 5′-adenylyl β,γ-imidodiphosphate or the nucleoside sangivamycin crystallized as a monomer. The C-terminal tail (C-tail) of AGC kinase domains is a highly conserved feature that is divided into three segments as follows: the C-lobe tether, the active-site tether (AST), and the N-lobe tether (NLT). This domain is fully resolved in GRK5 and reveals novel interactions with the nucleotide and N-lobe. Similar to other AGC kinases, the GRK5 AST is an integral part of the nucleotide-binding pocket, a feature not observed in other GRKs. The AST also mediates contact between the kinase N- and C-lobes facilitating closure of the kinase domain. The GRK5 NLT is largely displaced from its previously observed position in other GRKs. Moreover, although the autophosphorylation sites in the NLT are >20 Å away from the catalytic cleft, they are capable of rapid cis-autophosphorylation suggesting high mobility of this region. In summary, we provide a snapshot of GRK5 in a partially closed state, where structural elements of the kinase domain C-tail are aligned to form novel interactions to the nucleotide and N-lobe not previously observed in other GRKs.

The G protein-coupled receptor kinase (GRK)[3] family dates back to the discovery of rhodopsin kinase (GRK1) and now includes seven members that fall into the following three subfamilies: GRK1 (GRK1 and -7), GRK2 (GRK2 and -3), and GRK4 (GRK4–6) (1–3). GRKs are best known for their ability to phosphorylate activated G protein-coupled receptors (GPCRs) and promote arrestin binding, a process that drives receptor desensitization and trafficking as well as arrestin-mediated signaling (1–3). GRKs also phosphorylate many other proteins and can mediate kinase-independent regulation of receptor and effector function (2). Although most GRKs are localized in the cytoplasm or at the plasma membrane, GRK5 and GRK6 are also found in the nucleus with GRK5 localization being regulated by G_q signaling (4, 5) and GRK6 localization regulated by palmitoylation (6). These findings suggest many novel ways whereby GRKs may mediate their biological effects.

GRKs have been implicated in many pathological conditions, including cardiovascular disease, cancer, and various neurological and metabolic disorders (2, 3). This has been best studied in cardiovascular disease where increased GRK expression is associated with congestive heart failure, hypertension, and myocardial ischemia. GRK2 appears to play a particularly important role in this process and is overexpressed in human heart failure and hypertension as well as in experimentally induced heart failure models (7–9). GRK5 is also linked with cardiovascular disease and contributes to cardiac hypertrophy (10) and hypertension (11). Moreover, a Q41L polymorphism within the regulator of G protein signaling homology (RH) domain in GRK5 is prevalent in African Americans and has an enhanced ability to desensitize the β_2-adrenergic receptor (β_2AR) (12) and protect against the development of congestive heart failure (13). GRK5 has also been linked with type 2 diabetes (14), prostate tumor

* This work was supported, in whole or in part, by National Institutes of Health Grants R01 GM044944 and P01 HL114471 (to J. L. B.). This work includes work carried out at the Sidney Kimmel Cancer Center X-ray Crystallography and Molecular Interactions facility, which is supported in part by NCI Cancer Center Support Grant P30 CA56036. The authors declare that they have no conflicts of interest with the contents of this article.
◆ This article was selected as a Paper of the Week.
The atomic coordinates and structure factors (codes 4TNB and 4TND) have been deposited in the Protein Data Bank (http://wwpdb.org/).
[1] To whom correspondence may be addressed. Tel.: 215-503-4587; E-mail: anshul.bhardwaj@jefferson.edu.
[2] To whom correspondence may be addressed. Tel.: 215-503-4607; E-mail: jeffrey.benovic@jefferson.edu.

[3] The abbreviations used are: GRK, G protein-coupled receptor kinase; AGC, protein kinase A, G, and C families; CaM, calmodulin; β_2AR, β_2-adrenergic receptor; RH, RGS homology; AMP-PNP, 5′-adenylyl β,γ-imidodiphosphate; PIP_2, phosphatidylinositol 4,5-bisphosphate; SEC, size-exclusion chromatography; AUC, analytical ultracentrifugation; GPCR, G protein-coupled receptor; r.m.s.d., root mean square deviation; PDB, Protein Data Bank; BisTris, 2-[bis(2-hydroxyethyl)amino]-2-(hydroxymethyl)propane-1,3-diol; AST, active-site tether; NLT, N-lobe tether; KD, kinase-dead.

growth (15) and metastasis (16), Parkinson disease with dementia (17), synuclein phosphorylation and aggregation in sporadic Parkinson disease (18), and Alzheimer pathology in mice and humans (19), possibly due to its role in neurite outgrowth, learning, and memory (20). Taken together, these studies reveal that GRK5 is implicated in many different human diseases and may provide an important therapeutic target in the treatment of cardiovascular disease, neurological and metabolic disorders, and cancer.

Although it is important to understand the *in vivo* function of GRKs, it is also important to understand the mechanisms that mediate GRK function. Significant insight into GRK function has come from detailed biochemical and biophysical analysis. This has included defining important functional domains, including detailed mapping of interfaces such as GRK2 interaction with $G\alpha_q$ (21) and $G\beta\gamma$ (22) and GRK5 interaction with Ca^{2+}/calmodulin (23). Such studies have been greatly complemented by x-ray crystallography, and structures for GRK1 (24), GRK2 (25), GRK2/$G\beta_1\gamma_2$ (25, 26), GRK2/$G\beta_1\gamma_2$/$G\alpha_q$ (27), and GRK6 (28) have provided important insight. These structures reveal that the RH, catalytic, and C-terminal domains are in extensive contact and help to hold the kinase domain in an inactive open conformation. Several studies suggest that an N-terminal α-helical domain plays an important role in regulating catalytic domain closure via a process that is likely regulated by receptor binding (29–31). Indeed, this domain has been observed in one crystal form of GRK1 (24, 31) as well as in GRK6 in complex with either sangivamycin or AMP (30) and appears to stabilize catalytic domain closure. Although crystallography has provided significant insight on GRK1, -2, and -6, there have been no studies to date on the structural analysis of GRK5.

Here, we use x-ray crystallography to better understand the structure and function of GRK5. We find that human GRK5 shares significant structural similarity to other GRKs, albeit with some unique aspects. In contrast to crystal structures of GRK1 and GRK6, GRK5 is a monomer in the crystal and contains a well ordered kinase domain C-tail that includes interactions between the active-site tether and bound nucleotide. Such studies have high significance for understanding GRKs and how structure/function changes might mediate pathological consequences. Moreover, these studies should set the stage for developing strategies to specifically regulate GRK5 function in the treatment of disease.

Experimental Procedures

Materials—Sangivamycin, ADP, AMP-PNP, and phosphatidylcholine (soybean type II-S) were purchased from Sigma, and [γ-^{32}P]ATP was from PerkinElmer Life Sciences. Crystallization screening reagents were purchased from Hampton Research (Aliso Viejo, CA).

Protein Expression and Purification—The site-specific mutants GRK5-K215R and GRK5-R470A were generated using the QuikChange site-directed mutagenesis kit (Agilent) and verified by DNA sequencing. The Bac-to-Bac Baculovirus Expression System (Invitrogen) was used to generate baculoviruses to express human full-length wild-type GRK5, GRK5-R470A, and kinase-dead GRK5-K215R in Sf9 insect cells. The recombinant proteins were purified as described previously with some modifications (32). Briefly, cells were harvested by low speed centrifugation 48 h after infection, and the cell pellet was resuspended in lysis buffer (20 mM Hepes, pH 7.2, 250 mM NaCl, 5 mM EDTA, 1 mM phenylmethylsulfonyl fluoride, 10 μM leupeptin, 3 mM benzamidine, and 0.02% Triton X-100). Cells were lysed using a Brinkman Polytron (two times for 30 s at 25,000 rpm) followed by high speed centrifugation to remove cell debris. The supernatant was diluted 4-fold with buffer A (20 mM Hepes, pH 7.2, 2 mM EDTA, 0.02% Triton X-100, 1 mM dithiothreitol (DTT)) and applied to an SP-Sepharose cation-exchange column. The column was washed and eluted with a 50–750 mM linear NaCl gradient in buffer A. GRK5 peak fractions were pooled, diluted with buffer A, loaded onto a heparin-Sepharose 6 FF affinity column, and eluted with a 200–800 mM linear NaCl gradient in buffer A. GRK5-containing fractions were pooled, diluted with buffer B (20 mM Hepes, pH 7.2, 1 mM DTT), and injected onto a 1-ml Mono S cation-exchange FPLC column. Proteins were eluted with a 200–700 mM NaCl linear gradient in buffer B, and fractions containing GRK5 were combined, diluted to 200 mM NaCl with buffer B, concentrated in a 50-kDa molecular mass cutoff filter (Millipore Corp.) to ~20 mg/ml, aliquoted, and stored at −80 °C. The yield of pure GRK5 was 2–5 mg/liter of Sf9 cells with protein purity >95% as analyzed by SDS-PAGE.

Crystallization—Prior to crystallization, 8 mg/ml GRK5 (~120 μM) was incubated for 2 h with 4 mM AMP-PNP and 2 mM $MgCl_2$ (GRK5·AMP-PNP complex) or 0.4 mM sangivamycin and 0.2 mM $MgCl_2$ (GRK5·sangivamycin complex). Initial robotic screening for crystallization conditions was performed in a 96-well format using crystallization kits from Hampton Research. Protein droplets were prepared by mixing 0.4 μl of protein sample with 0.4 μl of reservoir solution and equilibrating against 60 μl of reservoir solution as a sitting drop at 4 °C. Several conditions under which crystals appeared were further optimized using the hanging-drop vapor-diffusion method and increasing the droplet size and reservoir volume by 5–8-fold, varying the concentration of precipitants and salts at different pH values. The complexes crystallized under similar conditions (AMP-PNP: 0.2 M NaCl, 0.1 M BisTris, pH 6.5, 20% w/v PEG 3350; sangivamycin: 0.15 M NaCl, 0.1 M BisTris, pH 5.5, 21% w/v PEG 3350). The best single diffracting crystals were obtained by micro-seeding. GRK5 crystals appeared within 3 days and grew over the course of 2–3 weeks with tetragonal bipyramidal morphology. SDS-PAGE analysis of a dissolved crystal revealed full-length GRK5. Crystals were cryoprotected using the reservoir solution supplemented to 35% PEG 3350 and flash-frozen in liquid nitrogen.

Data Collection, Structure Determination, and Refinement—Diffraction data for crystals were collected at beamline X6A at the Brookhaven National Synchrotron Light Source (NSLS) on an Area Detector System Corp. Quantum-270 detector using an x-ray wavelength of ~1.0 Å and 0.2° oscillations under a constant stream of liquid nitrogen maintained at 100 K. The best crystals for GRK5·AMP-PNP and GRK5·sangivamycin complexes diffracted to 1.8 and 2.1 Å, respectively. Diffraction data for both datasets were processed and scaled to primitive tetragonal space group $P4_32_12$ using HKL2000 suite (Table 1)

(33). The ligand-bound structures of GRK5 were solved by molecular replacement with Phaser (34) using two fragments of the GRK6 crystal structure (PDB code 2ACX) as the search model, corresponding to residues 30–179 and 180–507 (kinase domain). One copy of the GRK5 molecule was located in the asymmetric unit, which results in an estimated solvent content of ~43%. The model was subjected to iterative cycles of positional refinement and isotropic B-factor refinement using five TLS groups in Phenix.refine (35) as well as manual model building using Coot (36). To ascertain N-terminal residues 15–23 and a few loop regions of the model, omit-maps and feature-enhanced maps were calculated using PHENIX. Mg^{2+} ion, AMP-PNP, and sangivamycin were refined into their corresponding electron density as identified by difference maps. The final refined models for GRK5·AMP-PNP and GRK5·sangivamycin have R_{work}/R_{free} of 17.2/20.4 and 16.8/23.1%, respectively (Table 1). The R_{free} set was calculated using randomly selected reflections over 14 thin resolution shells. MolProbity (37) evaluation of main chain geometry suggests that >98.3% of residues occupy favored regions of the Ramachandran plot, with no outliers. The validity of refined structure models to the unmerged diffraction data was assessed using the correlation coefficient of half-datasets, CC*, using PHENIX. Also, CC*, CC_{work}, and CC_{free} were calculated for the final deposited structures in PHENIX and suggest that the structures were not over-fitted (Table 1) (38). Coordinates were deposited in RCSB structure database with PDB accession codes 4TND and 4TNB for GRK5·AMP-PNP and GRK5·sangivamycin complexes, respectively.

Structure Analysis—Structural superpositions were performed using the secondary structure matching algorithm in Coot (36, 39) and PDBeFold server (39) along with r.m.s.d. calculations and distance deviation analysis between regions. Domain hinge analysis was carried out using program DynDoM (40). All ribbon diagrams and surface representations in this work were generated using PyMOL (41). Nonlinear Poisson-Boltzmann electrostatic calculations were performed using APBS Tools plugin in PyMOL (42). Angles among superimposed regions were calculated using phenix.angle script of PHENIX 1.9–1692 (43). GRK5 intramolecular interactions and interactions with ligand were mapped using Ligplot plus (44) and PDBePISA server (80).

Analytical Ultracentrifugation—GRK5 was diluted in 20 mM Hepes, pH 7.2, 200 mM NaCl, 1 mM DTT to a concentration of 15 μM and subjected to analytical ultracentrifugation analysis in a Beckman ProteomeLab XL-I analytical ultracentrifuge in sedimentation velocity mode. GRK5 (400 μl) and reference buffer (420 μl) were loaded into a two-sector 1.2-cm path length Epon centerpiece sample cell. The runs were performed at fixed speed of 50,000 rpm^{-1} at a constant temperature of 4 °C, and absorbance values were collected at a fixed wavelength of 276 nm. The partial specific volume of GRK5 ($\bar{\nu}$), solvent density, and relative viscosity values in buffer solution along with theoretical molecular mass were calculated using SEDNTERP Version 1.09 (45). The resulting data were fitted to a continuous $c(s)$ distribution model in program SEDFIT (46) and an estimated molecular mass was obtained. The fitted data were visualized and presented using program GUSSI (University of Texas Southwestern).

Size-exclusion Chromatography—The apparent molecular mass of GRK5 was analyzed by size-exclusion chromatography on a Superose 12 16/60 column in 20 mM Hepes, pH 7.2, 200 mM NaCl, 1 mM DTT. The column was calibrated using protein standards for cytochrome *c* (12.4 kDa), carbonic anhydrase (29 kDa), albumin (66 kDa), alcohol dehydrogenase (150 kDa), β-amylase (200 kDa), and blue dextran (2000 kDa) from the gel filtration molecular weight markers kit (Sigma).

Circular Dichroism—Thermal unfolding of GRK5 and ligand-bound complexes was monitored by recording variations in ellipticity at 223 nm as a function of temperature in 1.0 °C increments from 20 to 70 °C using a Jasco J-810 spectropolarimeter equipped with a Peltier temperature control system. GRK5 at a final concentration of 5 μM was measured using a 0.1 cm quartz cuvette (Starna Cells, Inc.) in phosphate-buffered saline solution (3.2 mM Na_2HPO_4, 0.5 mM KH_2PO_4, pH 7.4, 135 mM NaCl), 0.4 mM ligand, 2 mM $MgCl_2$, and 0.4% dimethyl sulfoxide.

GRK5 Autophosphorylation Assays—Autophosphorylation of GRK5 and GRK5-K215R was detected using [γ-^{32}P]ATP. GRK5 and GRK5-K215R at concentrations of 0.12 and 0.6 μM, respectively, were incubated for 2 or 60 min in 20 mM Tris-HCl, pH 7.4, 5 mM $MgCl_2$, 30 mM NaCl, 0.5 mM EDTA, 100 μM [γ-^{32}P]ATP (2000 cpm/pmol), and 0.85 mg/ml soybean phosphatidylcholine vesicles at 30 °C. Reactions were stopped by addition of SDS loading buffer, and samples were run on SDS-PAGE, and the gel was stained with Coomassie Blue, dried, and visualized by autoradiography.

Michaelis-Menten Kinetic Analysis—K_m, V_{max}, and k_{cat} values for ATP were determined by varying ATP concentrations from 2 to 200 μM in reactions containing 10 μM rhodopsin (bleached for 5 min) and either 50 nM WT GRK5 or GRK5-R470A in 20 mM Tris-HCl, pH 7.4, 5 mM $MgCl_2$, 30 mM NaCl, 0.5 mM EDTA, and 4000 cpm/pmol [γ-^{32}P]ATP. Reactions proceeded for 2 min at 30 °C in room light and were stopped with SDS sample buffer. Rhodopsin phosphorylation was quantified by measurement of ^{32}P incorporation into rhodopsin after SDS-PAGE as described previously (32). Reaction velocities at the various ATP concentrations were fit to the Michaelis-Menten equation using GraphPad Prism.

Results and Discussion

Crystal Structure of GRK5—Previous studies suggest that the crystallization of ligand-free GRKs is very difficult because only an ~8 Å crystal structure of apo-GRK1 has been reported (24). Thus, we initially focused on using nucleotides to stabilize GRK5 and facilitate crystallization. Circular dichroism was used to investigate the structural stability of apo- and nucleotide-bound GRK5. Thermal unfolding of ligand-free GRK5 yielded an apparent melting temperature (T_m) of 31.5 °C, although the addition of nucleotides such as ADP, AMP-PNP, and sangivamycin resulted in an increase in T_m, consistent with stabilization (Fig. 1*A*). Sangivamycin, a potent nucleoside inhibitor of protein kinases (47), increased the T_m by 5.5 °C (T_m = 37 °C), ADP by 2.5 °C (T_m = 34 °C), AMP-PNP by 1.5 °C (T_m = 33 °C), and AMP had no effect (T_m = 31.5 °C). Thus, sangivamycin bind-

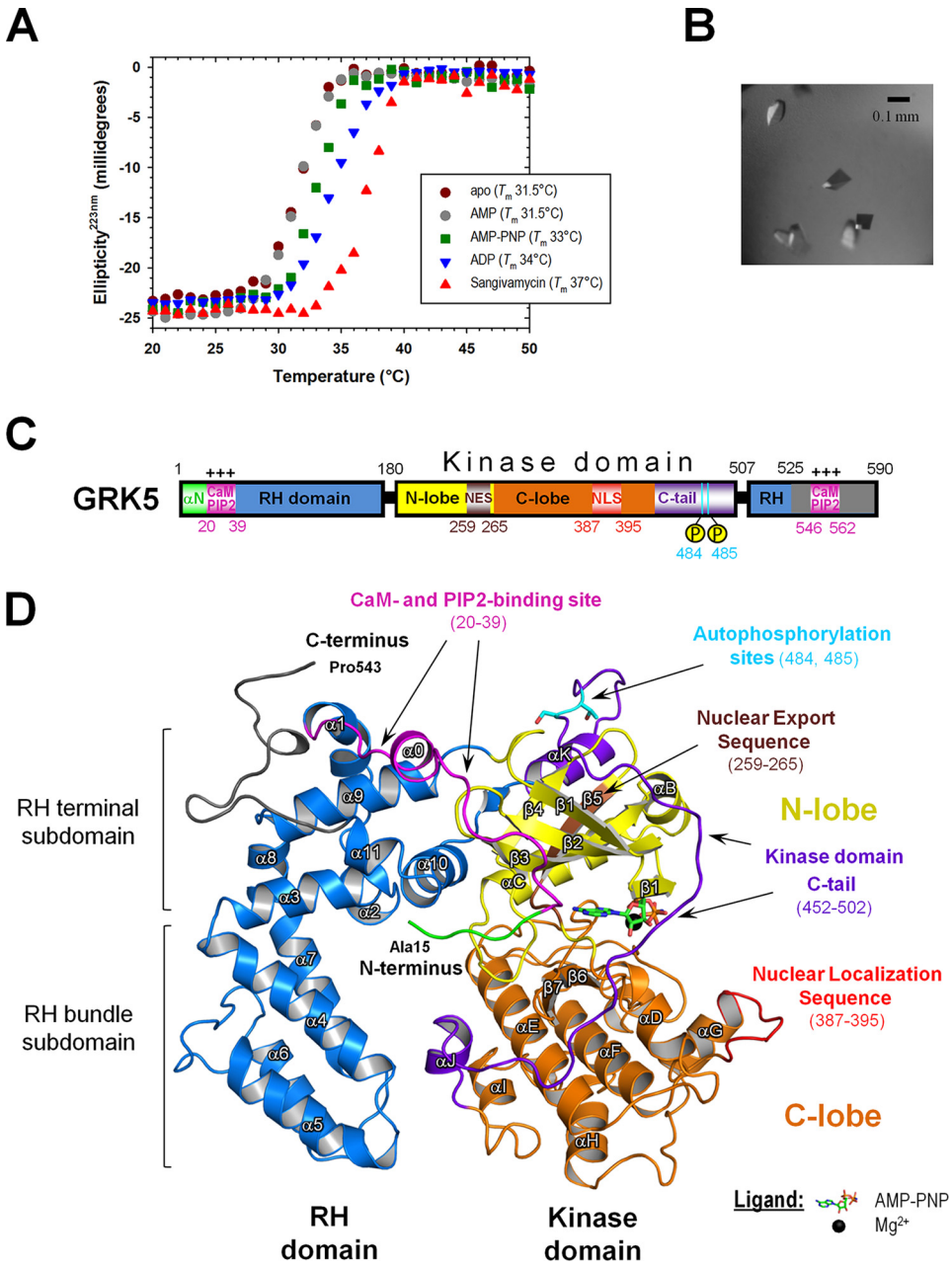

FIGURE 1. **Atomic structure of GRK5.** *A,* thermostabilization of GRK5 induced by different ligands. Stability of GRK5 against thermal denaturation was monitored by circular dichroism measurement of changes in the ellipticity intensity at 223 nm as a function of temperature. The measurements were performed at 5 μM GRK5 in the absence (apo-GRK5) or presence of 0.4 mM ligand. *B,* GRK5·AMP-PNP·Mg^{2+} crystals were grown at 4 °C to dimensions 0.04 × 0.04 × 0.12 mm. The crystals show bipyramidal morphology in contrast to rod-like thin plate crystals of its close homolog GRK6 (28). *C,* domain organization and important functional regions of GRK5. The RH domain is shown in *blue*, the catalytic domain in *yellow* (N-lobe) and *orange* (C-lobe), and the C-tail of kinase domain in *purple*. The two clusters of positively charged residues at the N and C terminus encompass GRK5 CaM- and PIP_2-binding sites (*magenta*). N-terminal amphipathic α-helix is in *green*. Autophosphorylation sites on the C-tail of the kinase domain are indicated by *yellow circles*. *D, ribbon* representation of GRK5·AMP-PNP crystal structure. Full-length GRK5(1–590) was crystallized, and residues 15–543 are clearly resolved (the first and last residues are labeled). The color coding is the same as in *C*. AMP-PNP ligand and Mg^{2+} are shown as *sticks* and *black sphere*, respectively.

ing induces significant stabilization of GRK5, whereas the effect of other nucleotides was less prominent.

Screening full-length human GRK5·AMP-PNP and GRK5·sangivamycin complexes led to diffracting crystals of tetragonal bipyramidal morphology (Fig. 1*B*). The data collection and refinement statistics are listed in Table 1. Structures of AMP-PNP and sangivamycin-bound GRK5 were solved to 1.8 and 2.1 Å resolution, respectively, and refined to R_{work}/R_{free} values of 17.2/20.4% (GRK5·AMP-PNP) and 16.8/23.1% (GRK5·sangivamycin) at given resolution. Both ligand-bound complexes were crystallized with nearly identical unit cell dimensions, crystal packing arrangement, and space group. The domain organization of GRK5 includes N-terminal α-helical, calmodulin/PIP_2 binding and RH domains, a central kinase domain, and a C-terminal region that includes a portion of the RH domain and a second calmodulin/PIP_2 binding domain (Fig. 1*C*). The crystal structures revealed a refined model lacking 14 N-terminal and 47 C-terminal residues with residues 15–543 clearly resolved,

TABLE 1
Crystallographic data collection and refinement statistics

	GRK5·AMP-PNP	GRK5·sangivamycin
Data collection statistics		
X-ray source	NSLS beamline X6A	NSLS beamline X6A
X-ray detector	ADSC Q270 CCD	ADSC Q270 CCD
Wavelength (Å)	1.0	0.98
Space group	$P4_32_12$	$P4_32_12$
Resolution (Å)	50.00–1.80 (1.83–1.80)[a]	50.00–2.1 (2.14–2.10)
Unit cell dimensions (Å)	$a, b = 62.975, c = 292.644$	$a, b = 62.676, c = 292.201$
Angles	$\alpha, \beta, \gamma = 90.0$	$\alpha, \beta, \gamma = 90.0$
Solvent content (%)/V_M (Å^3/Da)	43.8/2.19	43.1/2.16
Molecules/asymmetric unit	1	1
Total reflections	1,877,337	164,745
Unique reflections	52,751 (1625)	28,355 (525)
Multiplicity	35.6 (7.9)	5.8 (1.3)
Completeness (%)	94.2 (59.7)	81.7 (31.5)
Mean $I/\sigma(I)$	50.81 (1.17)	13.06 (1.03)
Wilson B-factor (Å^2)	26.48	29.75
R_{merge}[b]	0.09155 (0.8292)	0.122 (0.502)
R_{meas}[c]	0.0928 (0.905)	0.132 (0.668)
R_{pim}[d]	0.015 (0.292)	0.049 (0.437)
$CC_{½}$[e]	1.0 (0.762)	0.994 (0.643)
Refinement statistics		
Resolution (Å)	47.73–1.802 (1.867–1.802)	47.57–2.113 (2.188–2.113)
No. of reflections	1,876,659 (34,381)	164,708 (1716)
Reflections used for R_{free}	2459	1999
CC*[e]	1.0 (0.91)	0.998 (0.902)
R_{work}	0.1719 (0.2474)	0.1677 (0.2270)
R_{free}[f]	0.2037 (0.2839)	0.2307 (0.3362)
CC_{work}[e]	0.969 (0.823)	0.971 (0.836)
CC_{free}[e]	0.960 (0.853)	0.937 (0.738)
No. of non-hydrogen atoms	4832	4710
Macromolecules	4290	4290
Ligand	32	22
Water	510	398
Protein residues	529	529
Root mean square deviations from ideal geometry		
Bond length (Å)	0.008	0.008
Angles (°)	1.20	1.20
Ramachandran plot and MolProbity validation[g]		
Residues in favored region (%)	98.3	98.5
Residues in allowed region (%)	1.7	1.5
Residues as outliers (%)	0	0
Clash score	4.30	7.68
Overall score	1.21	1.42
Average B-factor (Å^2)		
Model (all atoms)	36.1	36.60
Protein	35.63	36.60
Ligand	32.80	25.83
Water	39.90	37.30
Mg^{2+} ion	42.34	
PDB code	4TND	4TNB

[a] Statistics for the highest resolution shell are shown in parentheses.
[b] The simple merging R factor for the multiple observations is shown (75, 76).
[c] Redundancy-independent merging R factor is shown (77).
[d] Precision-indicating merging R factor is shown (78).
[e] The $CC_{½}$ is the correlation coefficient between two randomly selected half-datasets; CC* is a statistic metric for assessing the effective resolution limits of data and quality of unmerged data in the context of a refined model; CC_{work} and CC_{free} are the standard and cross-validated correlations of the observed intensities to the refined model-based intensities, for the work and test sets, respectively (38).
[f] R_{free} value is calculated using the small subset of randomly selected reflections (test-set) that are set aside prior to refinement and not used in the refinement of the structural model (79).
[g] Data are from Chen *et al.* (37).

including the kinase domain C-tail, which is not visible in most GRK structures (Fig. 1*D*). Mass spectroscopic analysis reveals that the GRK5 used in crystallography is intact and lacks any post-translational modifications except for some very minor phosphorylation at the extreme C terminus (data not shown). This reveals that the N- and C-terminal regions missing from the structure are disordered and suggests high flexibility of these regions, a property common to most GRK crystal structures.

Overall, the crystal structures of AMP-PNP and sangivamycin-bound GRK5 were nearly identical (r.m.s.d. 0.35 Å), with minor changes in the structural arrangement of the kinase-active site (discussed below). This is in strict contrast to GRK6 (70.4% sequence identity to GRK5), which adopts distinct conformations in the presence of AMP-PNP (28) and sangivamycin (r.m.s.d. 1.94 Å) (30). The observed difference between GRK5 and GRK6 is likely dictated by structural restraints imposed by crystal contacts, which appeared to be ligand-independent in

the GRK5 complexes with AMP-PNP and sangivamycin, although the GRK6 complexes crystallized in two distinct packing arrangements and space groups. However, the minor differences between the two crystal structures of GRK5 may not reflect the propensity of the kinase to adopt distinct conformations in solution, because crystal structures often trap the lowest energy and most stable protein conformation. The absence of structural restraints imposed by crystal lattice contacts provides the necessary dynamics in the GRK5 molecule in solution resulting in significant differences in GRK5 stabilization induced by different ligands (Fig. 1*A*). However, because both structures show a high degree of structural identity and likely trap the most stable conformation of GRK5, we focused our analysis and discussion on the higher resolution GRK5 structure co-crystallized with the nonhydrolysable ATP analog AMP-PNP.

The GRK5 crystal structure contains features typical for protein kinases in general and GRKs in particular. The kinase domain possesses a bilobal-fold with a smaller N-terminal lobe (N-lobe, *yellow*) and a larger C-terminal lobe (C-lobe, *orange*) (Fig. 1*D*). The N-lobe consists of a canonical five-strand antiparallel β-sheet (denoted $\beta1$–$\beta5$) forming characteristic groove and flanking helices αB and αC. The GRK5 C-lobe is composed of a two-strand antiparallel β-sheet ($\beta6$-$\beta7$), located under the interlobe hinge region, and six α-helices (αD–αI). Fully ordered AMP-PNP is coordinated within the kinase interlobe cleft, representing the kinase-active site. Regulatory C-terminal extension of the kinase domain (Fig. 1*D, purple*) is fully ordered in GRK5 and is found in a position near the RH domain that has not been observed previously in other GRKs.

The bilobal architecture is also a characteristic feature of GRK RH domains that are structurally related with the regulator of G protein-signaling proteins (48). One lobe is composed of helices $\alpha4$–$\alpha7$ packed in an antiparallel manner to assemble the GRK5 RH bundle subdomain (Fig. 1*D*). The GRK5 RH terminal subdomain (second lobe) is by N-terminal helices $\alpha0$–$\alpha3$, $\alpha8$–$\alpha9$, and C-terminal $\alpha10$–$\alpha11$. The RH bundle and terminal subdomains generate a characteristic V-shaped notch with two ends forming a contact surface with adjacent kinase domain N- and C-lobes. The $\alpha10$-helix of the RH terminal subdomain has a large interface with the kinase N-lobe, whereas hydrophilic residues in the N-terminal ends of $\alpha4$ (backbone oxygen of Val^{92}) and $\alpha7$ (Lys^{139} and Glu^{140}) interact with the kinase domain C-lobe via polar contacts with Asn^{452}, Lys^{454}, and Arg^{455} of the αJ helix (at the beginning of the kinase domain C-tail). Thus, the RH and kinase domains of GRK5 are in intimate contact and establish a close relationship between the two domains that provides a structural basis for allosteric effects (*e.g.* receptor binding and kinase domain closure).

No domain-swapped interface, as is observed in prior structures of GRK1 and GRK6, was observed in GRK5, and both ligand complexes crystallized as a monomer in the asymmetric unit. The C-terminal calmodulin- and PIP_2-binding domain (residues 546–565) (23, 49, 50) is located within the disordered C-terminal segment, immediately adjacent to the last residue observed in the structure (Pro^{543}). Thus, this domain appears to be located near the $\alpha1$-helix of the RH domain and the N-terminal calmodulin/PIP_2-binding region (residues 20–39, colored *magenta* in Fig. 1, *C* and *D*) (23, 51). This suggests close proximity of these two important domains that mediate GRK5 interaction with phospholipids and calmodulin.

A noticeable divergence in the crystal structures of GRK5 and other GRKs is also observed in the relative position of the RH and kinase domains. The long axis of the RH and kinase domain of GRK5 is twisted compared with GRK1, GRK2, and GRK6 (Fig. 2). DynDoM analysis reveals that the hinge for this motion is located within the interdomain loop of GRK5 that connects the $\alpha9$-helix of the RH domain and the $\beta1$-sheet of the kinase domain (Fig. 1*D*). When the kinase domains are superimposed, the RH bundle subdomain demonstrates larger displacement than the RH terminal subdomain, consistent with the position of the RH bundle subdomain far distant of the hinge. It moves by ~10 Å on average ($\alpha6$ helix) relative to its position in other GRKs (the kinase domains are superimposed in Fig. 2). The significance of this observed movement of the two major domains of GRK5 is not clear, because it mainly affects the relative arrangement of the RH bundle and kinase C-lobe domains, regions that are remote from the predicted membrane- and receptor-binding surfaces. Moreover, no significant rearrangement of the contact interface between the RH and kinase domains of GRK5 was identified, and the individual structures of the RH subdomains were also changed very little (r.m.s.d. 0.4–0.9 and 1.4–1.6 Å for terminal and bundle, respectively, compared with GRK1 and GRK6). This movement is also unlikely to be related to the crystallization of GRK5 as a monomer, because a GRK1-L166K mutant that crystallized in a monomeric form lacks this structural feature (52). Interestingly, the 2.4 Å crystal structure of bovine GRK5 in complex with the GRK-selective inhibitor CCCG215022 (see accompanying paper (81)) also does not have the RH and catalytic domain rotation observed in our GRK5·AMP-PNP and GRK5·sangivamycin structures. This suggests some degree of structural plasticity in the relative orientation of these two major domains of GRK5.

GRK5 Is a Monomer Both in the Crystal Structure and in Solution—GRK1 and GRK6 crystallized as dimers in the asymmetric unit with the C termini of each molecule mediating a domain-swapped dimer interface (24, 28, 30). In contrast, GRK5 is a monomer in the crystal structure. Sequence alignment identified a unique Pro^{529} in the C-terminal region of GRK5 that is not present in other GRKs (Fig. 3*A*). Pro^{529} causes a kink in the polypeptide chain of the C terminus and bends it back upon itself. Thus, the direction of the visible segment of the C terminus (the fragment between Asn^{530} and the last visible residue Pro^{543}) is changed preventing antiparallel alignment of the C termini, which were found to stabilize the dimer interface in other GRKs. Arg^{169} is at a key position to support this architecture and packs against the C-terminal portion of GRK5 with its guanidinium group forming hydrogen bonds with the side chain of Asp^{536}, Asn^{525}, and the backbone oxygen of Val^{526}. In addition, residues Met^{165}, Phe^{166}, and Arg^{169} form a hydrophobic pocket to sandwich Phe^{527} instead of mediating a dimer interface as observed in GRK6 (28). A similar packing arrangement was found in GRK1-L166K, where dimerization was disrupted by mutation of Leu^{166} in the hydrophobic dimer interface resulting in GRK1 crystallization as a monomer (52).

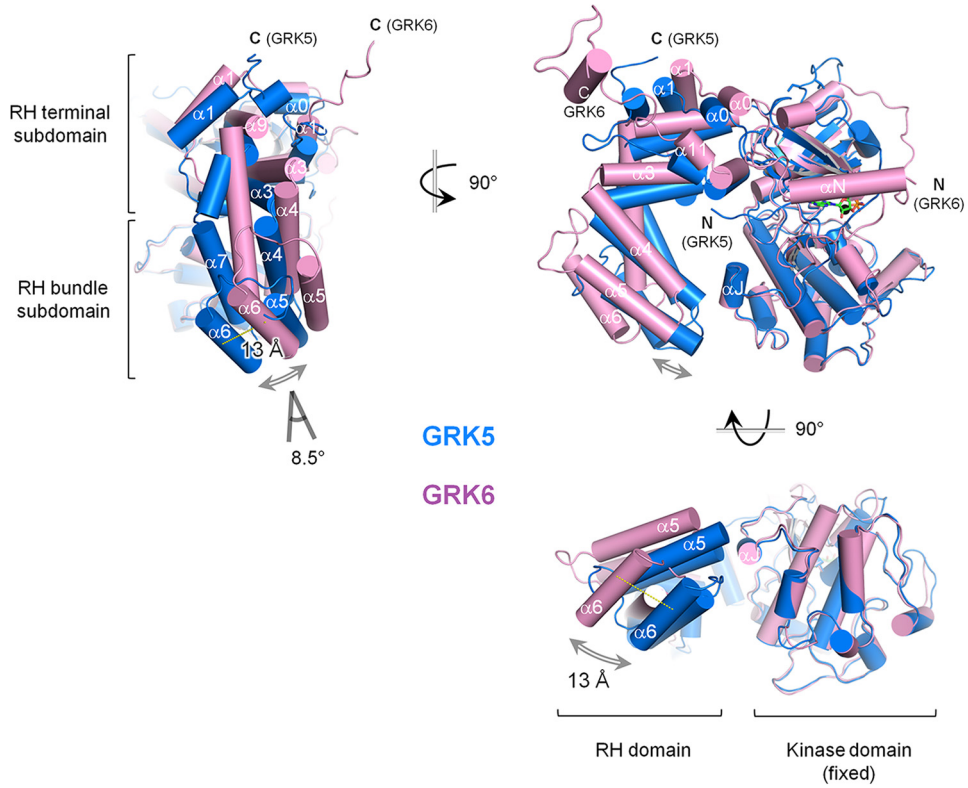

FIGURE 2. **RH domain displacement in GRK5.** Comparison of the structural topology of the RH and kinase domains in GRK5·AMP-PNP and GRK6·sangivamycin (PDB code 3NYN). Kinase domains were superimposed to reveal an 8.5° rotation of RH domain. The comparison of GRK5 with the GRK1 and GRK2 crystal structures reveals similar displacements of structural elements within RH domain with largest changes in the RH bundle subdomain (6–13 Å of α6-helix displacement) (data not shown).

This confirms that this topology of the C terminus promotes crystallization of a monomeric form of GRKs.

To determine whether GRK5 also exists as a monomer in solution, we performed size-exclusion chromatography (Fig. 3*B*) and analytical ultracentrifugation (AUC) (Fig. 3*C*). These experiments revealed molecular masses of ~70 kDa by size-exclusion chromatography and ~62.4 kDa by AUC under sedimentation velocity mode, consistent with a monomeric state, and no dimer or aggregate forms were detected. There is also little evidence that other GRKs form dimers in solution, although some contain a domain-swapped dimer interface in the crystal structures (28). Although the crystal structure and in-solution analysis of GRK5 does not exclude dynamic self-association of GRK5 under some conditions, it demonstrates that the C-terminal domain-swapped dimer interface typical in other GRKs is unlikely to be formed in GRK5.

Although our studies suggest that GRK5 is primarily a monomer in solution, there are a few recent reports that GRK5 can also dimerize. For example, a recent study on the role of GRK5 dimerization in plasma membrane localization demonstrated that a M165E/F166E mutation disrupts GRK5 dimerization and results in GRK5 redistribution from the plasma membrane to the cytoplasm (53). Although Met^{165} and Phe^{166} mediate a hydrophobic dimer interface in GRK6 (28), they are involved in intramolecular stabilization with Phe^{527} in GRK5 (Fig. 3*A*). Although destabilization of this intramolecular interface might result in a change of membrane-binding properties of GRK5, the Xu *et al.* (53) study provides several additional lines of evidence supporting a role for GRK5 dimerization in plasma membrane binding. In addition, a role for GRK5 dimerization was also suggested in actin nucleation (20). Moreover, we find that GRK5 can undergo intermolecular autophosphorylation in the presence of phospholipids (see Fig. 6*B*), also supporting its ability to dimerize under certain conditions. Taken together, these studies suggest that GRK5 dimerization may be linked to phospholipid binding.

Kinase Domain of GRK5 Adopts a Partially Closed Conformation and Binds Ligands in the Canonical ATP-binding Pocket—In AGC kinases, the small and large lobes of the kinase domain are observed to "close" upon binding of nucleotides and substrate peptides, phosphorylation of the activation loop or, in PKA, complex formation between catalytic and regulatory subunits (54, 55). It is believed that the fully closed conformation of the kinase domain allows proper alignment of substrate and nucleotide in the active site needed for effective catalysis (56).

Superposition of GRK5 with its close homolog GRK6 and the prototypical AGC kinase PKA reveals an intermediate partially closed conformation of the GRK5 kinase domain (structural coordinates of kinase domain C-lobe were superimposed to observe differences in conformation of N-lobe, indicative of kinase domain closure) (Fig. 4*A*). GRK5·AMP-PNP adopts a more closed conformation compared with the open state of apo-PKA (PDB code 1J3H) and GRK6·AMP-PNP (PDB code 2ACX), yet it is somewhat less closed than the fully closed conformation of PKA (catalytic subunit of the holo tetrameric complex; PDB code 3TNP). The catalytic cleft of GRK5 is nota-

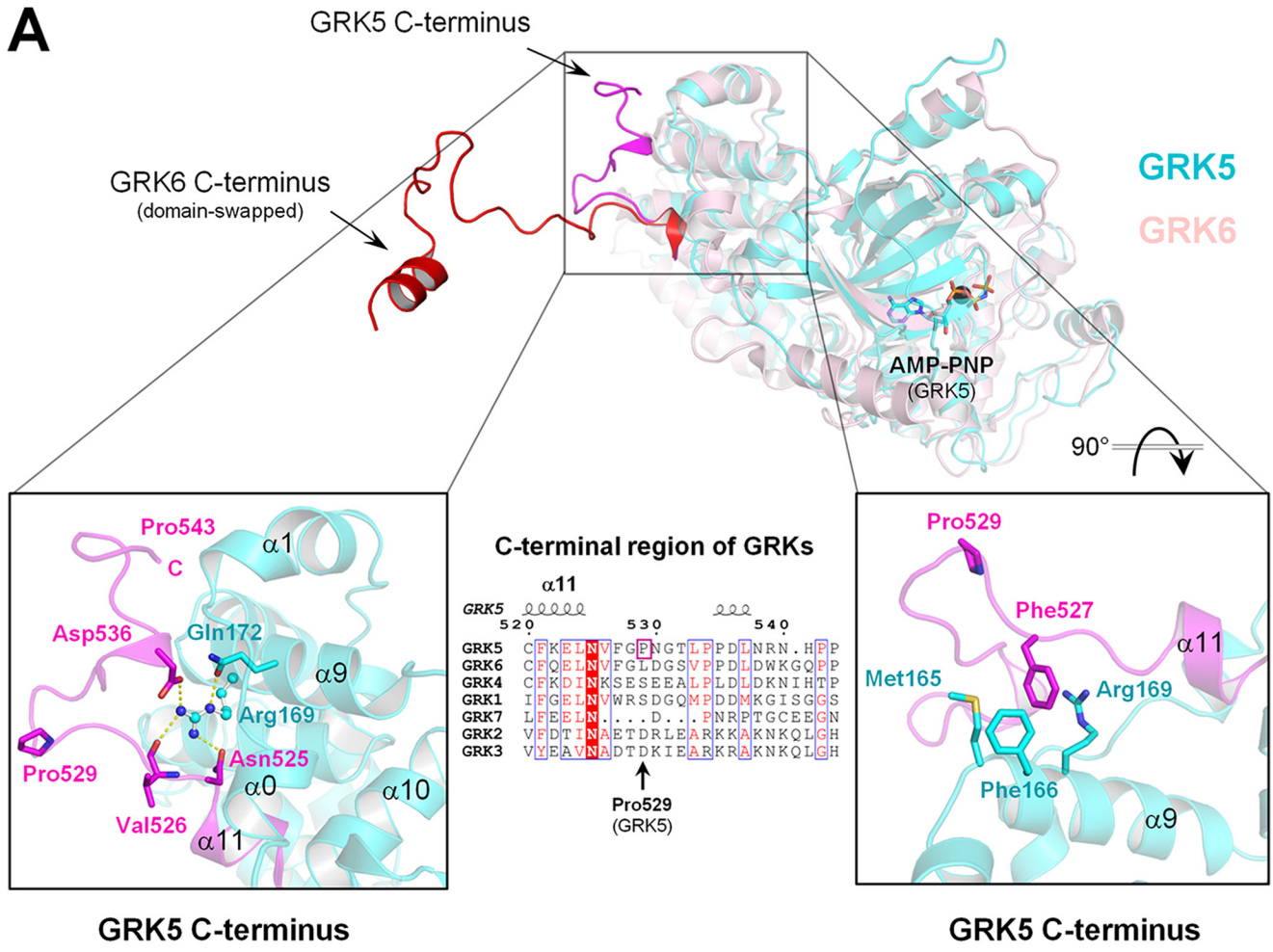

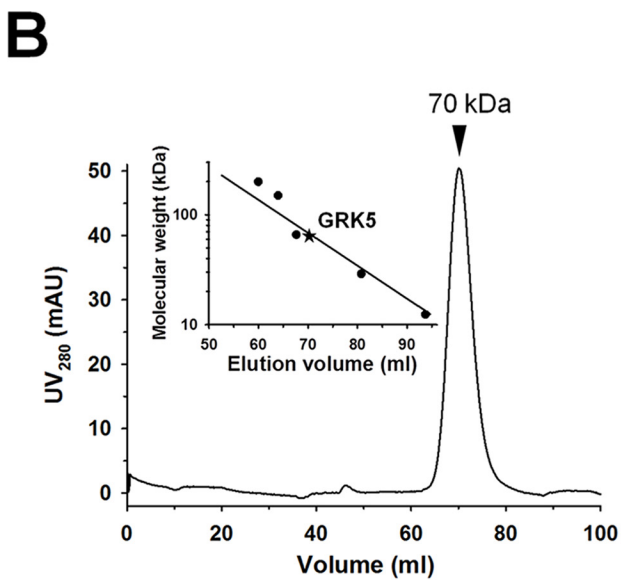

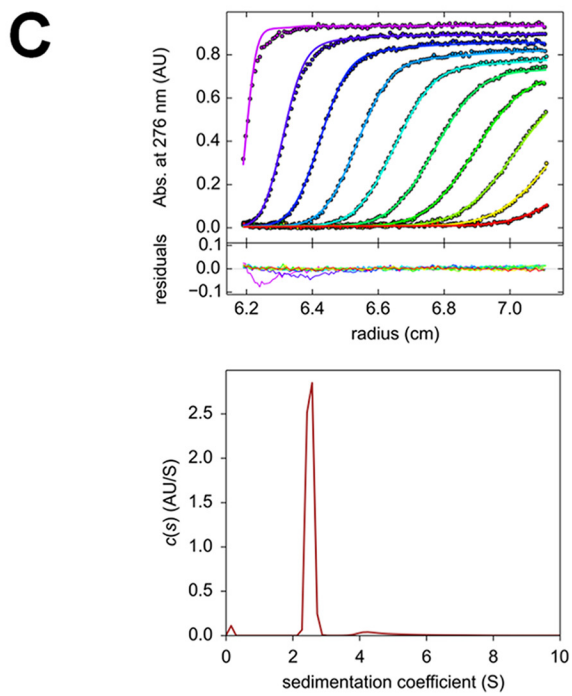

bly narrower than in apo-PKA and GRK6·AMP-PNP, consistent with a more catalytically competent conformation of the kinase domain. Overall, the conformation of the GRK5 kinase domain closely resembles the relatively closed state observed in the GRK6·sangivamycin structure (PDB code 3NYN), the most closed structure of a GRK determined to date.

AMP-PNP and sangivamycin both have strong electron density and low B-factors in the refined GRK5 structure. They reside in the canonical ATP-binding pocket in a large cleft formed in the interlobe space of the kinase domain. The purine ring of the ligands is buried within a hydrophobic pocket in the active site. Two additional conserved hydrogen bonds with Thr^{264} and Met^{266} of the hinge region fulfill binding for the adenine base (Fig. 4*B*). The triphosphate tail is more solvent-accessible than in the fully closed PKA structure (57) due to partial opening of the cleft and rising of the P-loop. The ribose portion of the ligand is partially shielded by a direct contact with the AST of the C-terminal extension of the kinase domain. The sangivamycin-binding site largely overlaps the adenine- and ribose-binding sites of AMP-PNP. AMP-PNP retains only one magnesium ion in a tridentate chelation by oxygen atoms of α-, β-, and γ-phosphates as well as Asp^{329} of the "DLG" motif ("DFG" in PKA/PKB/PKC) and Asn^{316} (Fig. 4*B*), similar to PKA·AMP-PNP (57) and PKB·AMP-PNP (58) structures, although magnesium ions are coordinated in a bidentate fashion by phosphate groups in this case. Magnesium also binds a catalytic water molecule to fulfill the octahedral coordination state (59). In the GRK6·AMP-PNP structure, Asp^{329} and Asn^{316} are displaced due to the more open conformation of the kinase domain and do not coordinate magnesium, although in the GRK5·sangivamycin complex, the side chain of Asp^{329} forms hydrogen bonds with the amide group at the C7 position of the diazaindole ring of sangivamycin instead of magnesium coordination.

One characteristic of the protein kinase active state is interaction between a conserved glutamate residue from the αC-helix and lysine residue from the β3-strand (60). Mutation of this catalytic lysine residue (Lys^{215} in GRK5/6, Lys^{216} in GRK1, and Lys^{220} in GRK2) into arginine inactivates GRKs. Lys^{215} is positioned by Glu^{234} to bind α- and β-phosphates of the ligand in GRK6·AMP-PNP and GRK1·ATP (Lys^{216} and Glu^{235}). In GRK5·AMP-PNP, Lys^{215} also forms a hydrogen bond with Glu^{234}, but it lacks contact with the triphosphate tail of the ligand (Fig. 4*C*). The triphosphate tail of AMP-PNP in GRK5 adopts a conformation with the α- and β-phosphates shifted 1.5 and 4 Å away from Lys^{215}, respectively, as compared with GRK6·AMP-PNP (28) and thus is less buried in the catalytic cleft (Fig. 4*C*). The crystal structure of GRK5·AMP-PNP was obtained under low magnesium concentration and therefore shows electron density for only one magnesium ion. As noted above, this magnesium ion is coordinated in a tridentate arrangement by the triphosphate tail in GRK5, although normally magnesium is coordinated in a bidentate manner by two phosphate groups of ATP or AMP-PNP. It is possible that the binding of a second Mg^{2+} (at high magnesium concentration) would change the triphosphate tail conformation and help to position it deeper in the active site cleft of GRK5, where it can interact with Lys^{215}.

The phosphate-binding glycine-rich loop (P-loop) of the N-lobe is formed by the β1-β2 turn and is directly engaged in binding of the triphosphate tail of ATP when the kinase is in its active state (full closure of kinase domain) and helps to stabilize the phosphorylation transition state (61). Because of incomplete closure of the kinase domain in GRK5, the P-loop is raised a bit above the triphosphate tail and is not fully engaged in phosphate group binding as observed in the fully closed conformation of PKA·AMP-PNP (57). P-loop is engaged in coordination of α- and β-phosphates, although it is still misaligned with the γ-phosphate. However, the P-loop of GRK5 is observed at a lower position when compared with the open conformations of apo-PKA (62) and GRK6·AMP-PNP (28). Interestingly, the P-loop of GRK5 seems to be in more intimate contact with the adjacent αB-helix of the N-lobe than in other GRK structures. Side chains of Glu^{218}, Arg^{221}, and Arg^{225} residues are situated on the side of αB-helix facing toward the P-loop and form a network of hydrogen bonds with the last two being directly bound to the backbone oxygen of Gly^{196} from P-loop (Fig. 4*D*). The adjacent residue Phe^{197} of the P-loop packs against the guanidinium group of Arg^{225} and is engaged in weak cation-π interaction. Overall, these contacts should stabilize the position of the P-loop. Compared with other GRKs, the interface between αB-helix and P-loop in GRK5 is stronger due to involvement of both arginines from the αB-helix, although in other GRKs the interaction is provided only by one Arg residue. The tight contact between the P-loop and the adjacent αB-helix of the N-lobe provides a basis for synergistic changes within these two sides of the kinase catalytic groove.

Active-site Tether Is an Integral Part of the Nucleotide-binding Pocket of GRK5—The C-terminal extension of the kinase domain (C-tail) is a conserved feature of all AGC kinases (63). It

FIGURE 3. **GRK5 is a monomer both in the crystal structure and in solution.** *A,* structural basis for monomeric state of GRK5. Atomic structures of GRK5·AMP-PNP (*cyan*) and GRK6·sangivamycin (chain A of dimeric complex PDB 3NYN is shown in *pink*) were aligned to highlight differences in the topology of the visible regions of their C termini. GRK5 is oriented from the top of the view in Fig. 1*D,* and its C terminus is shown in *magenta*, and the GRK6 C terminus is in *red*. The GRK6 C terminus is domain-swapped; its position is fixed by symmetry-related GRK6 molecule from the dimer complex (data not shown), and the GRK5 C terminus is aligned against its own RH domain. Key intramolecular contacts between the GRK5 C terminus and RH domain that support the specific architecture of the C terminus are highlighted in the *left box,* and the hydrophobic pocket consisting of Met^{165}, Phe^{166}, and Arg^{169} (RH domain) that retains Phe^{527} (C terminus) is highlighted in the *right box*. Sequence alignment of C-terminal regions of human GRKs indicates unique Pro^{529} (framed in *magenta*) that forms a kink, thereby hindering a domain-swapped interface in GRK5. Identical residues are *boxed in red,* and residues showing similarity are in *red* and grouped in a *blue frame*. *B,* size-exclusion chromatographic analysis of purified GRK5. A Superose 12 16/60 gel filtration column was calibrated using molecular mass markers, whose elution volumes and relative molecular masses were used to build a calibration curve (*inset*). GRK5 eluted as a single species consistent with an ~70-kDa monomeric state of the protein. *C,* sedimentation-velocity profile of GRK5. The *top panel* shows the raw absorbance (*solid circles*) collected at 276 nm with the interval of 40 min together with corresponding fitted data (*solid line*) plotted as a function of radial position. The low values (< 5% of signal) for residuals confirm fidelity of fit between raw and fitted data. The monophasic sedimentation boundaries suggest that GRK5 exists as a monodisperse single species in solution. The *bottom panel* shows the fitted distribution of the apparent sedimentation coefficient calculated for GRK5 is 2.6 S, which corresponds to an estimated molecular mass of ~62.4 kDa, consistent with a monomer of 67.8 kDa (theoretical molecular mass).

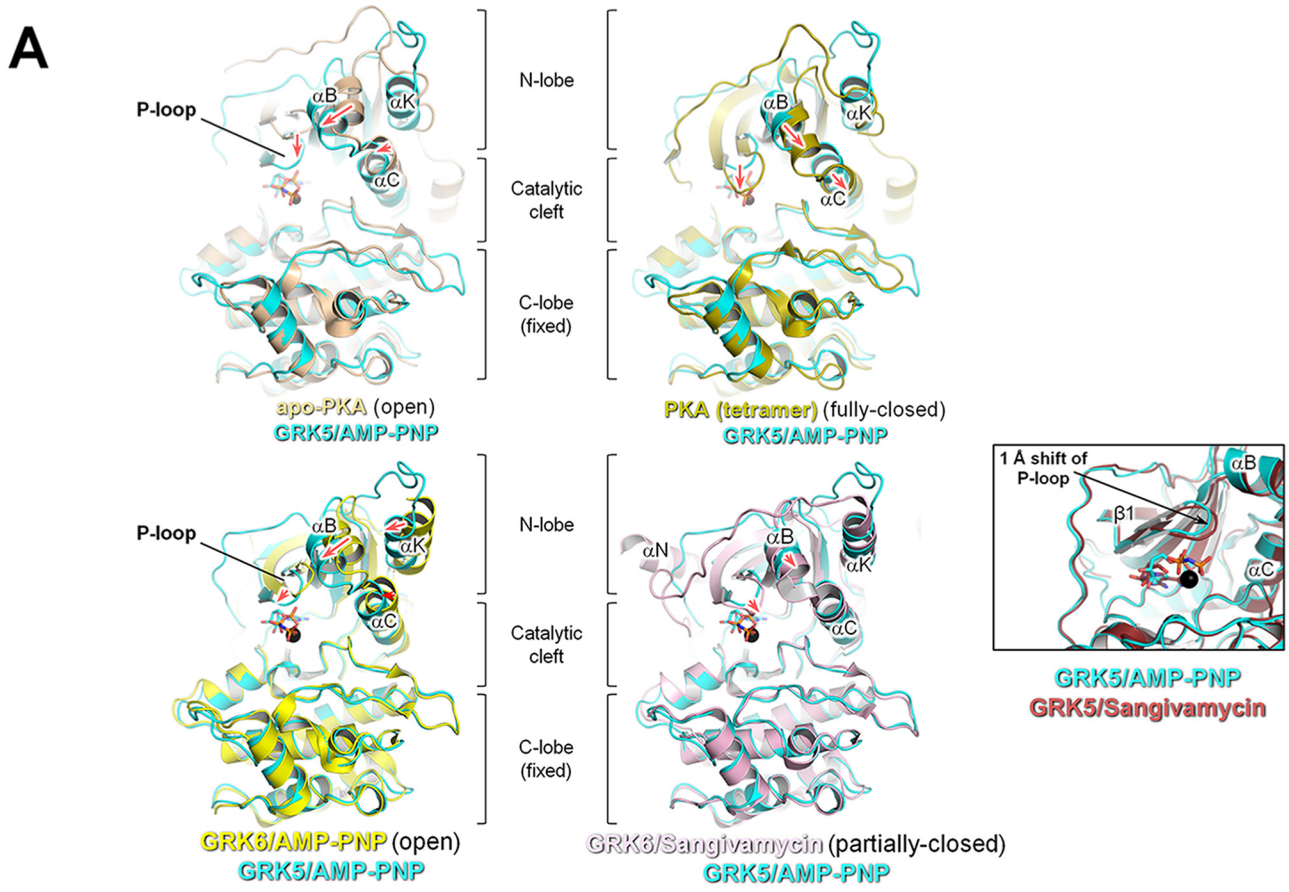

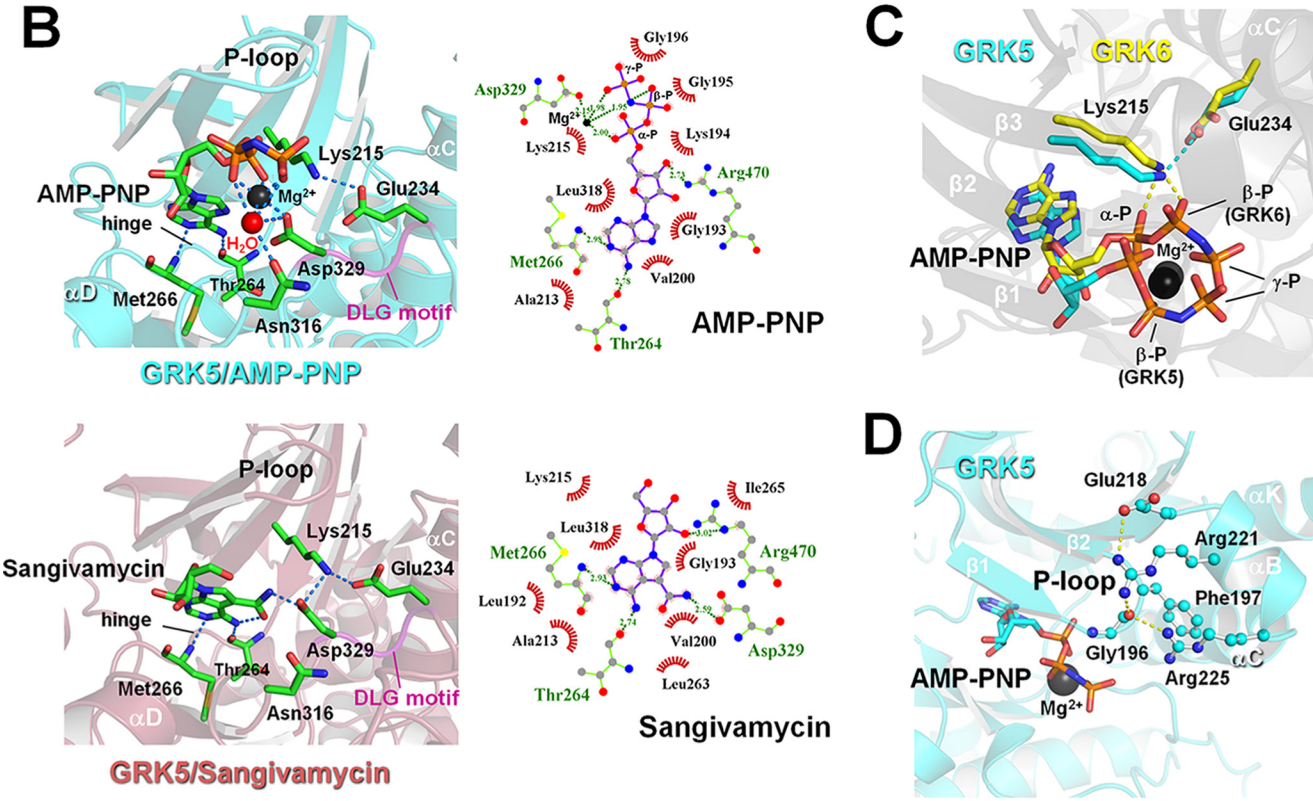

spans the kinase domain C-lobe (C-lobe tether; residues 451–467 in GRK5), active site (AST; residues 468–473), and N-lobe (N-lobe tether (NLT); residues 474–502) (Fig. 5*A*). The C-tail plays a regulatory role in AGC kinases, acting either as a cis-interacting regulatory element with direct influence on kinase activity or as a scaffold for trans-interacting elements that dock on the C-tail and modulate AGC kinase activity (63).

The AST segment of the C-tail regulates the catalytic cycle of substrate phosphorylation in AGC kinases and helps to control entry and exit of nucleotide in the kinase-active site (so-called "nucleotide gate") (54). It is typically disordered in the absence of nucleotide but becomes an integral part of the ATP-binding site when nucleotide is bound and the kinase domain is closed (64). A conserved Phe-Asp-Asp-Tyr (FDDY) motif (residues 327 to 330 in PKA) in the AST, particularly Phe^{327} and Tyr^{330}, is part of the hydrophobic pocket that anchors the adenine and ribose rings of ATP in PKA and many other AGC kinases (Fig. 5*B*) (63). Replacement of these residues with Ala reduces affinity for ATP and ultimately inactivates the enzyme (65, 66). In GRKs, the FDDY motif is not conserved, and the AST fragment does not coordinate nucleotide even when fully ordered as in the GRK6/sangivamycin structure (30). However, we observed a direct contact of the AST segment to the ribose ring of AMP-PNP and sangivamycin in GRK5, which resembles the AST-nucleotide interaction observed in PKA and PKB (Fig. 5*B*).

The AST spans the active site with the side chain of Arg^{470} intruding into the nucleotide-binding pocket of GRK5 to hydrogen bond with the ribose ring of AMP-PNP. Guanidinium group of Arg^{470} directly interacts with 3′-OH of the AMP-PNP ribose ring, although analogous interaction of Tyr^{330} of PKA requires an active-site conserved water molecule to mediate AST interaction with 2′-OH of the ribose ring (Fig. 5*B*). Importantly, Arg^{470} also mediates a hydrogen bond network and plays a central role in bridging the C-tail with the N-lobe (Arg^{470} backbone oxygen and guanidinium group interact with Arg^{190} and Leu^{192} of the β1-strand, respectively) and the hinge region (Arg^{470} backbone amide binds to Asn^{267}) (Fig. 5*C*). Although GRK5 adopts an intermediate state with the structural elements of the kinase domain not fully aligned for phosphotransfer, the contact interface between Arg^{470} and other parts of the kinase domain facilitate its closure. Interestingly, in the GRK6·sangivamycin structure, the ordered αN-helix and Arg^{190} of β1-strand were at the center of the interface stabilizing the closed state of the kinase domain (30). We speculate that Arg^{470} has a similar role in GRK5, which also adopts a partially closed conformation even in the absence of αN-helix ordering. Furthermore, Arg^{470} seems to have an even more prominent role in the GRK5·sangivamycin complex compared with GRK5·AMP-PNP, because its side chain is bent toward the C-lobe, and the guanidinium group also hydrogen bonds with Asp^{270} of C-lobe (Fig. 5*C*), in addition to the observed interaction to the ribose ring in the AMP-PNP complex. Thus, tighter contact between N- and C-lobes provided by AST in GRK5·sangivamycin might better stabilize the closed state of the kinase domain, which is in agreement with increased thermostability demonstrated in our biophysical studies (Fig. 1*A*). It might also explain the slight lowering of the P-loop in comparison with GRK5·AMP-PNP (Fig. 4*A*, *inset*), although the lack of phosphate groups in sangivamycin as compared with AMP-PNP is a more compelling argument in this case. Similar lowering of P-loop was observed in PKA complex with adenosine (similar to sangivamycin it lacks a triphosphate tail; PDB code 1FMO) as compared with PKA·AMP-PNP crystal structure (PDB code 4DH3).

Interestingly, despite a large sequence difference between the AST segments of PKA and GRK5, it maintains similar spatial arrangement of intramolecular contacts with nucleotide and N- and C-lobes (Fig. 5*D*). It appears that the guanidinium group of Arg^{470} in GRK5 occupies a similar locus as conserved catalytic water in PKA (*red sphere* in Fig. 5*D*), which was shown to form a network of interactions with nucleotide (links Tyr^{330} to 2′-OH of ribose ring), N-lobe (through the carbonyl oxygen of Leu^{49} of P-loop), and C-lobe (through the carboxylate of Glu^{127}) in a fully closed state of catalytic subunit in PKA. Similar interactions are observed in GRK5 but without assistance of the catalytic water molecule. Also, backbone carbonyl and amide of Arg^{470} in GRK5 form similar contacts with the hinge and the N-lobe as observed for Asn^{326} and Asp^{329} of the AST fragment in PKA (Fig. 5*D*). Thus, Arg^{470} in the GRK5 AST maintains a similar set of contacts as distinct AST residues in PKA. Structural conservation of these contacts in GRK5 suggests an essentially similar role of AST for kinase domain closure that was well characterized in PKA (59, 63).

To further assess a role for C-tail interaction with nucleotide in GRK5, we replaced Arg^{470} with alanine and compared catalytic parameters of mutant and wild-type GRK5. GRK5-R470A

FIGURE 4. **GRK5 kinase domain adopts a partially closed conformation.** *A,* structural alignment of the GRK5 kinase domain with the open, partially closed (intermediate), and fully closed conformations of the kinase domains from PKA (*top panel*) and GRK6 (*bottom panel*) reveals that the GRK5 kinase domain is in an intermediate, partially closed conformation. Structural coordinates of the kinase domain C-lobe were superimposed to reveal conformational changes in the N-lobe. The changes in the N-lobe that are indicative of kinase domain closure (αB, αC, αK, and P-loop) are shown with *red arrows*. Only AMP-PNP (*stick model*) from GRK5, which indicates active site of kinase, is shown. *Inset,* GRK5 in complex with AMP-PNP or sangivamycin (active site view) was aligned based on their C-lobes to highlight 1 Å lowering of P-loop (slightly more closed conformation) in the sangivamycin complex compared with the AMP-PNP complex. *B,* ligand-binding pockets for AMP-PNP and sangivamycin in GRK5. *Left panel,* view of catalytic cleft with residues that form ligand-binding site presented in *stick model*. The one magnesium ion (*black sphere*) is retained in tridentate manner by oxygen atoms of α-, β-, and γ-phosphates of AMP-PNP with the side chains of Asp^{329} (DLG motif) and Asn^{316} also involved in its coordination. The catalytic H_2O molecule that mediates Asn^{316} and Asp^{329} contact with Mg^{2+} and the triphosphate tail is shown as a *red sphere*. Nitrogen, oxygen and phosphorus atoms are colored *blue, red,* and *orange*, respectively. *Right panel,* two-dimensional schematic diagrams of GRK5 interactions with AMP-PNP and sangivamycin. Residues that form hydrogen bonds (*dotted lines*) with the ligands are shown in *ball-and-stick* with the interatomic distances shown in Å. The *spoked arcs* represent residues making van der Waals interactions with the ligand. Diagrams were generated with Ligplot plus. *C,* differences in conformation of triphosphate tail of AMP-PNP in crystal structures of GRK5 and GRK6 (PDB code 2ACX). The conserved residue Glu^{234} (αC-helix) hydrogen bonds with another conserved residue, Lys^{215} (β3-strand), in GRK5 and GRK6 (shown as *cyan dashed line* between GRK5 residues). Lys^{215} pairs with β-phosphate of AMP-PNP in GRK6 (*yellow dashed lines*), although β-phosphate in GRK5 is positioned far from Lys^{215}. *D,* P-loop/αB-helix binding interface in GRK5·AMP-PNP structure. Main chain oxygen of Gly^{196} (P-loop) is engaged in hydrogen-bonding network, including Arg^{225}, Arg^{221}, and Glu^{218} of αB-helix (N-lobe). Residues involved in the binding interface are shown in *ball-and-stick* representation, and AMP-PNP and Mg^{2+} are shown as *stick* and *black sphere*, respectively.

did not demonstrate a dramatic effect on Michaelis-Menten kinetics for ATP, albeit catalytic efficiency (k_{cat}/K_m) was reduced by 22% compared with WT GRK5 (Fig. 5*E*). Interestingly, the effect was primarily due to a change in V_{max} (K_{cat}), although the K_m value was unchanged. This suggests that the contribution of Arg^{470} to nucleotide binding is minimal (no effect on K_m), although it facilitates the GRK5 catalytic reaction (effect on k_{cat} and V_{max}). In agreement with this, a lower rate of substrate phosphorylation by GRK5-R470A was revealed in time courses of rhodopsin and tubulin phosphorylation by GRK5 (data not shown). Although a mechanistic understanding of this at the molecular level requires additional studies,

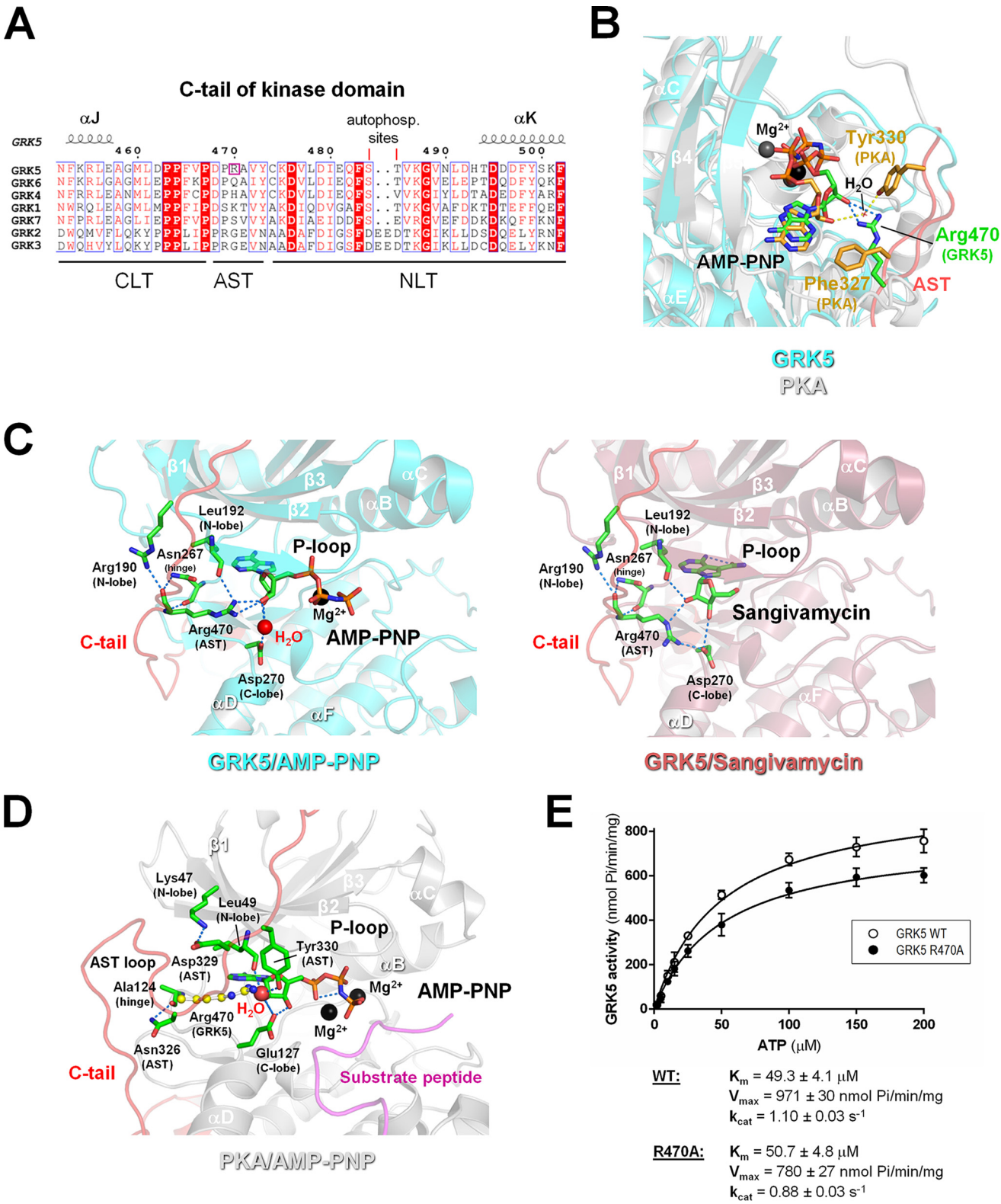

Arg^{470} interaction with the ribose ring might help to stabilize the orientation of nucleotide within the active site needed for effective catalysis. Another possible interpretation can be related to a potential role of Arg^{470} in facilitating ADP release, the rate-limiting step in product turnover by protein kinases (67). The AST is engaged in nucleotide coordination and is found in close proximity to the kinase-active site in fully closed (active) conformation of PKA, although it is further away from the active site in the intermediate and open states (68). Thus, the AST might provide an additional driving force for ADP release when the catalytic cycle is complete and the enzyme adopts a more open conformation with the AST moving away from the active site and pulling out the nucleotide from the kinase-binding pocket. If true, AST interaction with nucleotide should increase nucleotide off-rate, which is in agreement with observed higher catalytic turnover rate for ATP of WT GRK5 as compared with GRK5-R470A where AST is disengaged.

Thus, the kinase domain C-tail of GRK5 is fully ordered, and its AST fragment directly interacts with nucleotide in the catalytic cleft thereby playing a similar nucleotide gate role as in many other AGC kinases. In contrast, the AST in GRK1 (24) and GRK6 (28) is disordered and not part of the nucleotide-binding pocket, despite the active site being occupied with ADP or ATP (AMP-PNP). AST in GRK6·sangivamycin is ordered, mainly due to interactions with αN-helix, but it is not involved in coordination of the ligand. Available crystal structures of GRK2 lack electron density for nucleotide in the nucleotide-binding pocket, although GRK2-Gβγ was crystallized in the presence of ATP, and therefore, it is not clear whether the AST is involved in nucleotide coordination. However, the AST is partially ordered in a structure of GRK2 bound to the serotonin reuptake inhibitor paroxetine, mainly due to a few weak van der Waals contacts with the piperidine B ring of paroxetine (69). Thus, a role of AST in other GRKs is not clear. Interestingly, Arg^{470} is not conserved even within the GRK4 subfamily (His in GRK4 and Gln in GRK6, see GRK sequence alignment in Fig. 5*A*); therefore, the contribution of the AST in nucleotide coordination could be unique to GRK5.

Structural Mobility of the Kinase Domain C-tail—The kinase domain C-tail (Fig. 5*A*) is generally disordered to a different degree in GRK crystal structures and has only been completely modeled in partially closed GRK1·ATP (24) and GRK6·sangivamycin (30). Although the GRK5 crystal structure also adopts a partially closed state, there are marked differences in the position of the C-tail and its intramolecular contacts. The entire kinase domain C-tail of GRK5 is well ordered with consistently low B-factor values (32.0 $Å^2$ for the C-tail *versus* 35.6 $Å^2$ for an entire ligand-bound model, see Table 1) compared with the structures of GRK1 and GRK6 (data not shown). Extensive intramolecular and intermolecular (crystal packing) contacts account for the low B-factors of the C-tail in GRK5. Fragment 470–475 and αK-helix are stabilized through crystal contacts to the adjacent GRK5 molecule in the crystal lattice. The AST is also stabilized via hydrogen bonding to nucleotide, whereas the NLT is anchored in the binding pocket formed by β1–β5 strands of the N-lobe. Comparing its position relative to the N-lobe in GRK1 and GRK6, the GRK5 NLT, including the autophosphorylation sites, moves more than 20 Å away from the close proximity of the catalytic cleft and occupies a new position close to the RH domain (Fig. 6*A*). In GRK6·sangivamycin, the AST forms a typical "tail loop" (Fig. 6*A*, *inset*) interacting with αN-helix (which is disordered in GRK5). The tail loop ("AST loop") is not formed in GRK5, and instead of binding to the αN-helix, the AST region participates in nucleotide coordination with Arg^{470}. Moreover, unwinding of the tail loop results in displacement of AST residues upward from the kinase-active site (*e.g.* 12 Å shift of Tyr^{473} in GRK5 relative to its the N-lobe in GRK5 (29 amino acids, residues 474–502) as compared with GRK6 (23 amino acids, residues 480–502) and GRK1 (26 amino acids, residues 481–506). This enables the NLT to follow a novel path and be positioned inside the N-lobe β-sheet groove, a site that is not occupied in GRK1 and GRK6. This new position of the NLT resembles the position of the NLT in PKA/PKB/PKC, which also span the N-lobe groove, although the NLT is not as deeply buried as in GRK5.

The NLT in PKA/PKB/PKC serves as a docking site for an upstream kinase PDK1 that mediates PKA/PKB/PKC phosphorylation and positions the αC-helix within the ATP-binding pocket (63). In the GRK1 and GRK4 subfamilies, the NLT contains adjacent autophosphorylation sites that appear to regulate GPCR phosphorylation (Fig. 5*A*) (2). We examined the mobility of the NLT segment by analyzing intramolecular autophosphorylation of GRK5 (Fig. 6*B*). In addition, we also tested the ability of wild-type GRK5 (WT) to phosphorylate a kinase-dead

FIGURE 5. **AST is an integral part of the nucleotide-binding pocket of GRK5.** *A,* sequence alignment of human GRK kinase domain C-terminal extension. GRK5 autophosphorylation sites (Ser^{484} and Thr^{485}) are indicated as is Arg^{470} in the AST (*framed* in *magenta*), which forms a direct contact with the nucleotide in GRK5. Identical residues are *boxed* in *red,* and residues showing similarity are in *red* and grouped in a *blue frame*. *CLT*, C-lobe tether. *B,* interaction of AST with nucleotide in the active site of GRK5 and PKA as viewed from above the P-loop. Phe^{327} and Tyr^{330} (AST) mediate van der Waals interactions with the AMP-PNP purine and 2′-OH of the ribose ring (via active-site conserved water), respectively, in PKA, and the guanidinium group of Arg^{470} hydrogen bonds with the 3′-OH of AMP-PNP ribose ring in GRK5. The β1–β3 strands were removed for clarity. *C,* hydrogen bond network stabilized by Arg^{470} in GRK5 complexes with AMP-PNP and sangivamycin. Arg^{470} mediates interactions with the nucleotide (via ribose ring of AMP-PNP and sangivamycin), N-lobe (via Arg^{190} and Leu^{192}), hinge (via Asn^{267}), and C-lobe (via Asp^{270} in GRK5·sangivamycin). Thus, Arg^{470} likely plays an important role in the interface that promotes closure of the kinase domain and regulates nucleotide entry/exit. The GRK5·AMP-PNP structure lacks direct Asp^{270} (C-lobe) contact with Arg^{470} and ribose (mediated by catalytic water molecule in this case) that is observed in GRK5·sangivamycin and might explain the slightly less closed conformation of the kinase domain in GRK5·AMP-PNP. *D,* interactions within the catalytic site of PKA bound to AMP-PNP and substrate peptide (*magenta*) analogous to Arg^{470} in GRK5. Side chain of Arg^{470} is modeled in *yellow ball-and-stick* representation to show its position in GRK5 relative to PKA (kinase domains of GRK5 and PKA are aligned). Active site conserved water molecule (*red sphere*) that connects Tyr^{330} to the ribose ring of AMP-PNP in PKA hydrogen bonds with Leu^{49} (β1-strand of N-lobe) and the ribose ring hydroxyl group, thus resembling the guanidinium group of Arg^{470} interactions with Leu^{192} and 3′-OH of the AMP-PNP ribose in GRK5. Moreover, the AST/hinge and the AST/N-lobe contacts provided by backbone carbonyl and amide of Arg^{470} in GRK5 are similar to Asn^{326} (AST)/Ala^{124} (hinge) and Asp^{329} (AST)/Lys^{49} (N-lobe) contacts, respectively, in PKA. Thus, interactions of AST with the nucleotide and N- and C-lobes that help to stabilize the closed state of the kinase domain in PKA are arranged in a similar manner in GRK5 and PKA. *E,* effect of R470A mutation on Michaelis-Menten kinetics for ATP. The kinetic parameters were determined by incubating 50 nM GRK5, 10 μM rhodopsin, and 2–200 μM ATP as described under "Experimental Procedures." The data are derived from three experiments and fitted to Michaelis-Menten kinetics using GraphPad Prism.

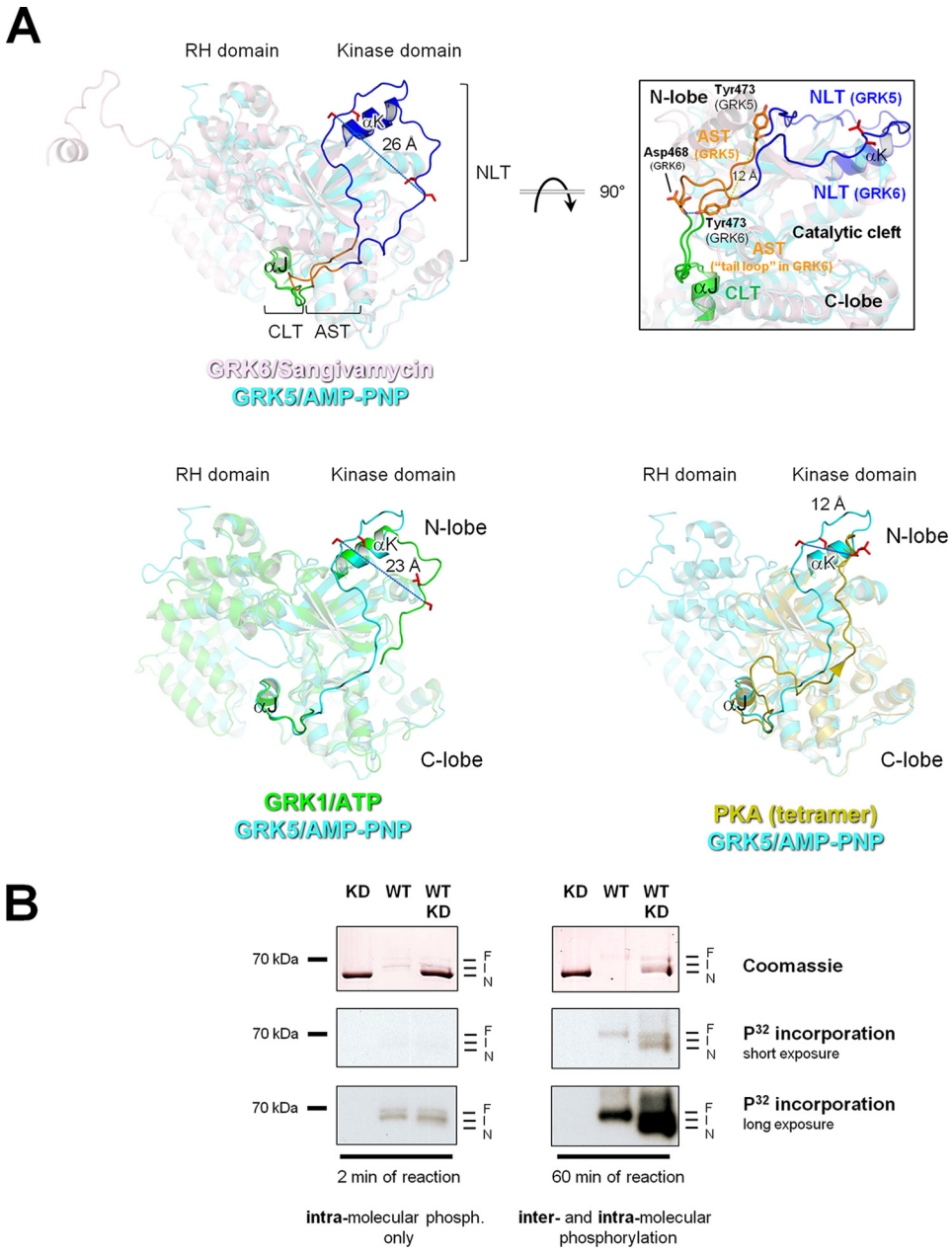

FIGURE 6. **Structural mobility of the kinase domain C-tail in GRKs.** *A,* comparison of kinase domain C-tail orientation in GRK5 relative to its position in GRK6 (PDB code 3NYN, *upper left*), GRK1 (PDB code 3C4W, *lower left*), and PKA (PDB code 3TNP, *lower right*) reveals a large displacement of the GRK5 NLT segment compared with GRK1 and GRK6. The GRK5 NLT moves away from the catalytic cleft and occupies a position close to the RH domain with autophosphorylation sites (*red sticks*) largely shifted from their position in GRK1 and GRK6 (23 Å and 26 Å, respectively). The structural coordinates of the GRK5 NLT more closely resemble the conformation of the NLT in PKA (12 Å distance between corresponding positions of autophosphorylation sites, Ser^{338} in PKA and Ser^{484} in GRK5). *Inset*, *upper right*, Tyr^{473}, which is conserved in the GRK1 and GRK4 subfamilies, forms a hydrogen bond with the backbone amide of Asp^{468} and stabilizes the tail loop (AST loop) in GRK6. In GRK5, Tyr^{473} shifts 12 Å away from its position in GRK6 and does not stabilize formation of the AST loop. *B,* GRK5 is autophosphorylated in an intra- as well as intermolecular manner. GRK5 (*WT*) and kinase-dead GRK5-K215R (KD) were autophosphorylated alone or in a WT/KD mixture at a 1:5 molar ratio. The reaction was done in the presence of [γ-^{32}P]ATP and phospholipid vesicles at 30 °C for 2 or 60 min as described under "Experimental Procedures." Only intramolecular autophosphorylation of WT GRK5 was observed after 2 min, which demonstrates the mobility of the GRK5 kinase domain C-tail, which can access the active site of GRK5 situated ~25 Å away from the catalytic cleft in the crystal structure. Phosphorylation of the KD mutant was only detected at 60 min when WT GRK5 was present, demonstrating the ability of GRK5 to autophosphorylate in an intermolecular manner. GRK5 that is fully autophosphorylated (*F*), intermediately autophosphorylated (*I*), or nonphosphorylated (*N*) is denoted on the *right*.

mutant GRK5-K215R (KD) to assess intermolecular autophosphorylation. In the presence of ATP and phospholipids, GRK5 undergoes rapid autophosphorylation at Ser^{484} and Thr^{485} within the NLT (70). KD and WT GRK5 were incubated separately or together for 2 or 60 min, and incorporation of ^{32}P into GRK5 was evaluated by SDS-PAGE. Autophosphorylated forms of GRK5 migrate slower, which leads to the appearance of two shifted bands of partially and fully autophosphorylated WT GRK5 after 2 min and one band of fully autophosphorylated WT GRK5 after 60 min. Only autophosphorylation of the WT enzyme was detected upon 2 min of reaction despite a 5-fold molar excess of KD GRK5, providing evidence for an

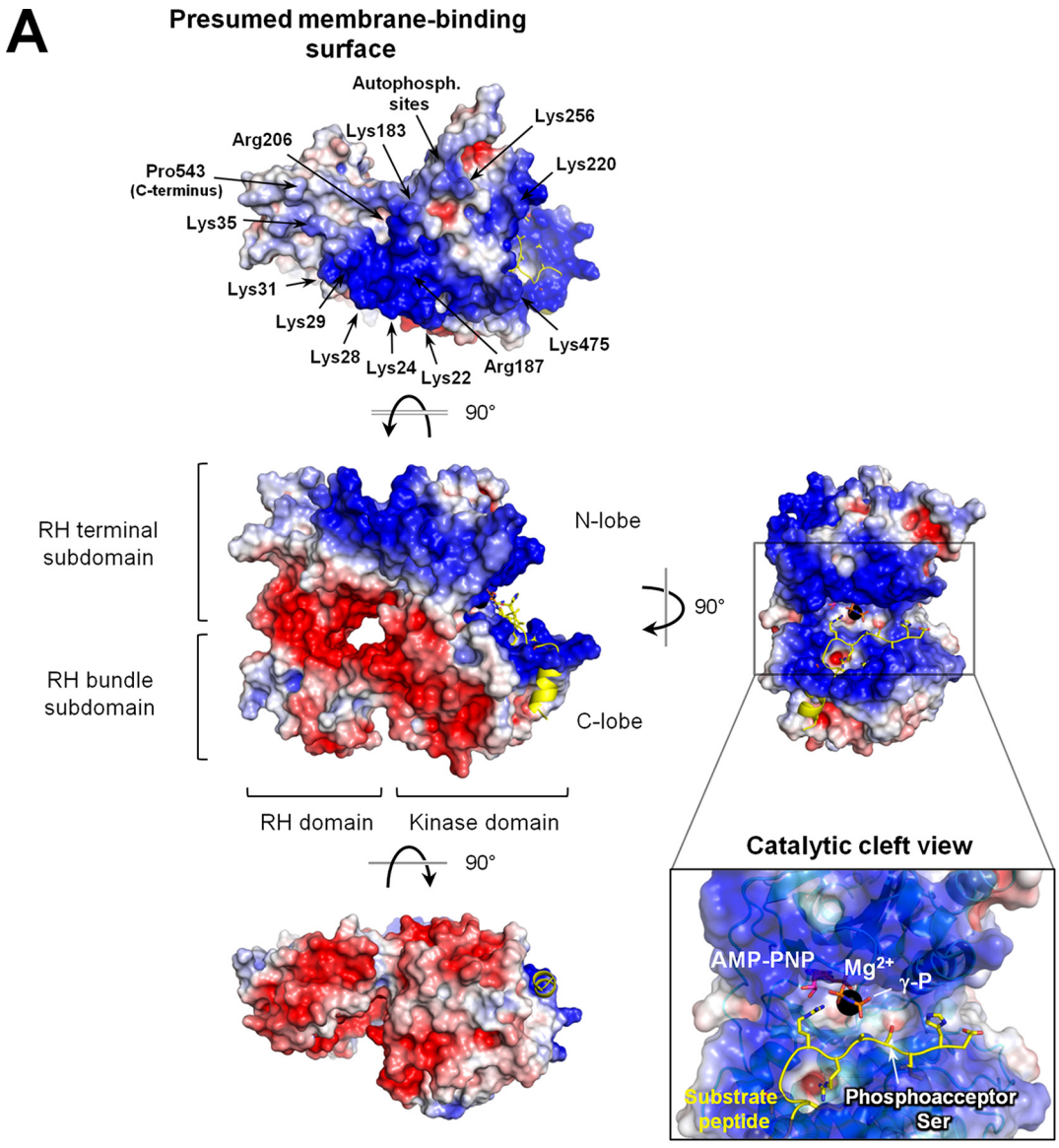

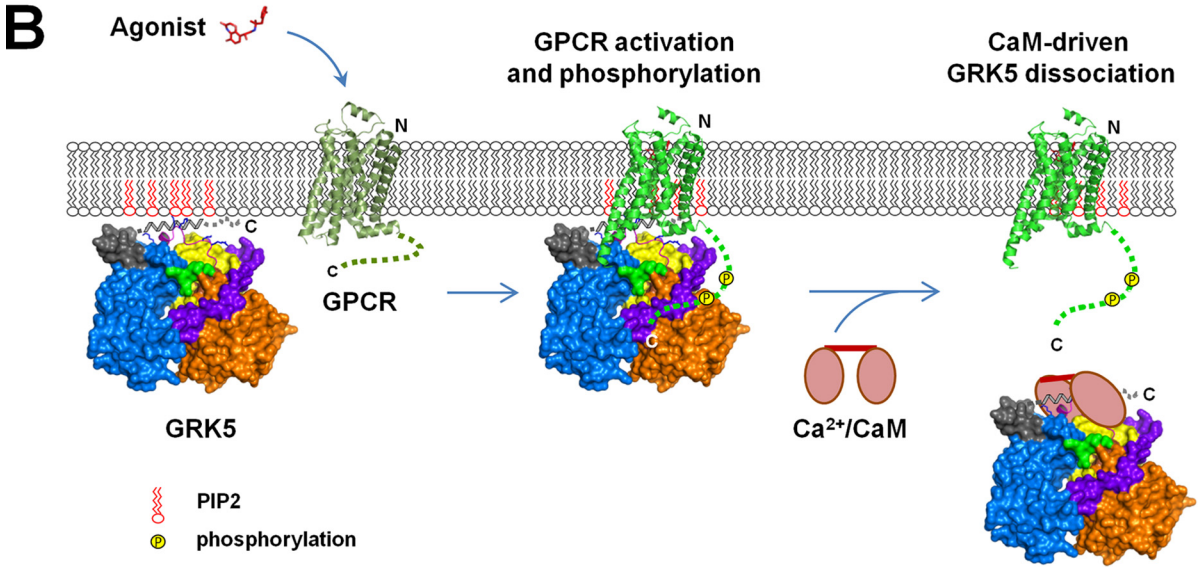

intramolecular reaction (Fig. 6*B*). The KD mutant is not capable of any autophosphorylation, and therefore its phosphorylation is indicative of intermolecular phosphorylation by WT GRK5. Phosphorylation of KD mutant was detected after 60 min suggesting that intermolecular phosphorylation of GRK5 also occurs, albeit with much slower kinetics than intramolecular autophosphorylation (Fig. 6*B*). Thus, autophosphorylation of GRK5 can occur in an intra- as well as an intermolecular manner (cis- and trans-autophosphorylation). Because autophosphorylation sites in the NLT are situated relatively far from the catalytic cleft in the crystal structure of GRK5, intramolecular autophosphorylation suggests high mobility of this region in solution. In the crystal structure, mobility of this region is restricted by crystal packing contacts, although conformational variability of the C-tail observed in different ligand complexes of GRKs (either fully or more often partially visible C-tail) also implies "malleability" of the C-tail.

Molecular Basis of GRK5 Association with the Plasma Membrane—Several mechanisms of membrane localization are utilized by GRKs to be in close proximity to their substrates, the integral membrane G protein-coupled receptors. These include C-terminal prenylation (GRK1 and GRK7), palmitoylation (GRK4 and GRK6), pleckstrin homology domain binding to acidic phospholipids and membrane-associated G$\beta\gamma$-subunits (GRK2 and GRK3), and electrostatic interaction with phospholipids (GRK4–6) (1). Two clusters of basic/hydrophobic residues within the N- and C-terminal regions appear to play a primary role in GRK5 association with phospholipids (Fig. 1*C*). When oriented as in Fig. 1*D*, an electrostatic contour reveals a bipartite distribution of the surface charge with the top (including N- and C-terminal regions) and the right side (N-lobe and catalytic cleft of kinase domain) of GRK5 abundant in basic residues, although the RH domain and C-lobe (except for its active site surface area) are predominantly negatively charged (Fig. 7*A*, *left center*). The N-terminal membrane-binding determinant (residues 22–35) is part of the positively charged area on the top of GRK5 and, together with several other basic residues in the N-lobe and the C-tail of kinase domain that lie in the same plane, constitutes a large membrane-binding surface (Fig. 7*A*). Based on the position of the last visible residue in the structure (Pro^{543}), the C-terminal membrane-binding determinant (residues 546–562) should be located in close proximity to the N-terminal membrane-binding interface and therefore extend the area of positive charge on the membrane-binding region of GRK5. Simultaneous anchoring of the N- and C-terminal basic regions might result in formation of a single broad surface that promotes stable association of GRK5 with phospholipids (Fig. 7*B*). Two-dimensional diffusion within the membrane plane would enable GRK5 to rapidly encounter and dock on an activated GPCR (Fig. 7*B*). This would be followed by kinase domain closure and proper alignment of the receptor phosphoacceptor sites (C terminus) onto the C-lobe of the catalytic cleft in a manner analogous to how substrate peptide docks into the catalytic cleft of PKA, which was used to model substrate binding for GRK5 in Fig. 7*A* (C-lobes of PKA and GRK5 were aligned). Once receptor phosphorylation is complete, GRK5 would likely dissociate from the receptor and possibly the membrane via a process that may be regulated by GRK5 autophosphorylation (Fig. 7*B*). This would be similar to GRK1, where autophosphorylation facilitates dissociation of GRK1 from phosphorylated rhodopsin (71).

Another aspect of GRK5 regulation to consider is its ability to interact with calmodulin (CaM), a ubiquitous Ca^{2+} sensor that links elevation of intracellular calcium levels with GRK inhibition. Although the exact mechanism of CaM binding to GRK5 is unknown, previous studies demonstrated that CaM binds to N- and C-terminal regions of GRK5 (residues 20–39 and 546–562) (23, 72), which largely overlap with the membrane-binding determinants. This leads to the hypothesis that CaM binding would block GRK5 association with membranes in response to elevation of intracellular calcium levels and thereby attenuate GPCR phosphorylation (Fig. 7*B*). Moreover, CaM enhances the redistribution of GRK5 from the plasma membrane to the cytoplasm and/or nucleus, where GRK5 targets a different set of substrates (5). CaM wrapping around an amphipathic α-helix of a target protein represents the canonical binding mode of CaM (73). Moreover, CaM can induce helical formation when bound to regions that were previously extended or disordered

FIGURE 7. **GRK5 electrostatic surface and a model for GRK5 binding to phospholipid membranes.** *A,* electrostatic surface potential of GRK5. The surface potential of GRK5 is depicted from −5 (*red,* acidic) to +5 (*blue,* basic) *kT/e*$^-$, and neutral regions are *white*. The stretch of basic residues is clustered on the top of GRK5 and maps the presumed membrane-binding surface. The N-terminal membrane-binding region (residues 22–35) is abundant in Lys residues (labeled) and is at the core of the interface providing electrostatic interaction of GRK5 with negatively charged lipids in the plasma membrane. A few positively charged residues of the N-lobe and the C-tail of kinase domain might also contribute to electrostatic anchoring of GRK5 on membranes. It should also be emphasized that although the C-terminal membrane-binding region (residues 546–562) is not resolved in the GRK5 crystal structure, it is near the last residue that was observed (Pro^{543}, labeled) and thus should be in the same plane with the N-terminal membrane-binding region likely constituting a common electrostatic surface for membrane attachment. The electrostatic contour of the kinase-active site also has a basic character. Substrate peptide (*yellow stick model*) from a PKA·AMP-PNP·SP20 complex (PDB code 4DG0) was mapped onto GRK5 C-lobe to model substrate binding into the catalytic cleft of GRK5 (coordinates of C-lobes of GRK5 and PKA were aligned). The zoomed-in view demonstrates the peptide orientation relative to AMP-PNP in GRK5. The site of phosphorylation on the substrate peptide is labeled and is positioned against the γ-phosphate of AMP-PNP. This illustrates the initial step of the kinase catalytic cycle (substrate and nucleotide alignment into the kinase-active site). *B,* structural model depicting binding and CaM-driven dissociation of GRK5 from phospholipid membrane and GPCRs. The model is based on the GRK5 crystal structure, which is oriented relative to the phospholipid surface in a manner that would bring the N-terminal membrane domain (residues 22–35) in close contact with PIP_2 in the plasma membrane. Color coding is the same as in Fig. 1*D*. The GRK5 C terminus (residues 544–590) is incomplete in the crystal structure and therefore unresolved regions are depicted as a *gray dashed line,* and the C-terminal membrane-binding region (residues 546–562) is depicted as a *gray* α-helix. The crystal structure of GRK5 suggests close location of both N- and C-terminal membrane-binding determinants implying that they can form a single interface and work synergistically to target GRK5 to the membrane. Binding of agonist to inactive GPCR (*light green*, from the crystal structure of β_2AR in complex with the inverse agonist ICI 118551, PDB code 3NY8) promotes GPCR activation. Docking of GRK5 on an activated GPCR (*green,* from the β_2AR·G_s complex structure, PDB code 3SN6) promotes full closure of the kinase domain and proper alignment of phosphoacceptor sites on the receptor (*green dashed line*). CaM and GRK5 autophosphorylation regulate the stability of GRK5 association to the membrane and GPCR. CaM (shown as a *brown model*) drives GRK5 redistribution from membrane compartment to cytoplasm or nucleus, where GRK5 targets a different set of substrates. GRK5 autophosphorylation sites (Ser^{484} and Thr^{485}) are located at the presumed GRK5/lipid bilayer interface in the crystal structure, and hence, autophosphorylation might change the electrostatic potential of GRK5 and destabilize GRK5 anchoring on the membrane.

(74). Although both CaM-binding regions on GRK5 have a propensity to form amphipathic α-helices as predicted by secondary structure simulation (data not shown), the N-terminal CaM-targeting region (residues 20–39) is largely unstructured (Fig. 1*D*). Moreover, it is also involved in extensive intramolecular contacts with RH domain residues. This includes Trp^{30}, a residue predicted to form an interface with CaM (72) that is buried within a hydrophobic pocket of GRK5 and is thus inaccessible to CaM. Thus, it is reasonable to speculate that binding of CaM to the N-terminal CaM-targeting region would involve a structural rearrangement within the N-terminal CaM-binding region that would include dissociation from the RH domain and subsequent helical formation induced by CaM binding.

Author Contributions—K. E. K. purified proteins, designed, performed, and analyzed all enzymatic, CD, and SEC experiments, prepared figures, and wrote the paper. A. B. and K. E. K. crystallized the complexes and carried out x-ray data collection and structural analysis. A. B. solved the crystal structures and performed AUC experiment and analysis and wrote the paper. J. L. B. conceived and coordinated the study and wrote the paper. All authors reviewed the results and approved the final version of the manuscript.

Acknowledgments—We thank Drs. Gino Cingolani and John Tesmer for helpful comments on the manuscript and Hsin-Yao Tang for mass spectrometry analysis and discussion. We are thankful to Vivian Stojanoff and the scientific staff at NSLS beamline X6A for assistance and help in data collection. Crystallographic data were collected at the X6A beamline of National Synchrotron Light Source, Brookhaven National Laboratory, which is funded by National Institutes of Health under agreement GM-0080 from NIGMS and the United States Department of Energy under Contract DE-AC02-98CH10886.

References

1. Krupnick, J. G., and Benovic, J. L. (1998) The role of receptor kinases and arrestins in G protein-coupled receptor regulation. *Annu. Rev. Pharmacol. Toxicol.* **38,** 289–319
2. Gurevich, E. V., Tesmer, J. J., Mushegian, A., and Gurevich, V. V. (2012) G protein-coupled receptor kinases: more than just kinases and not only for GPCRs. *Pharmacol. Ther.* **133,** 40–69
3. Premont, R. T., and Gainetdinov, R. R. (2007) Physiological roles of G protein-coupled receptor kinases and arrestins. *Annu. Rev. Physiol.* **69,** 511–534
4. Martini, J. S., Raake, P., Vinge, L. E., DeGeorge, B. R., Jr., DeGeorge, B., Jr., Chuprun, J. K., Harris, D. M., Gao, E., Eckhart, A. D., Pitcher, J. A., and Koch, W. J. (2008) Uncovering G protein-coupled receptor kinase-5 as a histone deacetylase kinase in the nucleus of cardiomyocytes. *Proc. Natl. Acad. Sci. U.S.A.* **105,** 12457–12462
5. Gold, J. I., Martini, J. S., Hullmann, J., Gao, E., Chuprun, J. K., Lee, L., Tilley, D. G., Rabinowitz, J. E., Bossuyt, J., Bers, D. M., and Koch, W. J. (2013) Nuclear translocation of cardiac G protein-coupled receptor kinase 5 downstream of select G_q-activating hypertrophic ligands is a calmodulin-dependent process. *PLoS One* **8,** e57324
6. Jiang, X., Benovic, J. L., and Wedegaertner, P. B. (2007) Plasma membrane and nuclear localization of G protein coupled receptor kinase 6A. *Mol. Biol. Cell* **18,** 2960–2969
7. Ungerer, M., Böhm, M., Elce, J. S., Erdmann, E., and Lohse, M. J. (1993) Altered expression of β-adrenergic receptor kinase and β1-adrenergic receptors in the failing human heart. *Circulation* **87,** 454–463
8. Gros, R., Benovic, J. L., Tan, C. M., and Feldman, R. D. (1997) G-protein-coupled receptor kinase activity is increased in hypertension. *J. Clin. Invest.* **99,** 2087–2093
9. Huang, Z. M., Gold, J. I., and Koch, W. J. (2011) G protein-coupled receptor kinases in normal and failing myocardium. *Front. Biosci.* **16,** 3047–3060
10. Gold, J. I., Gao, E., Shang, X., Premont, R. T., and Koch, W. J. (2012) Determining the absolute requirement of G protein-coupled receptor kinase 5 for pathological cardiac hypertrophy: short communication. *Circ. Res.* **111,** 1048–1053
11. Harris, D. M., Cohn, H. I., Pesant, S., and Eckhart, A. D. (2008) GPCR signalling in hypertension: role of GRKs. *Clin. Sci.* **115,** 79–89
12. Wang, W. C., Mihlbachler, K. A., Bleecker, E. R., Weiss, S. T., and Liggett, S. B. (2008) A polymorphism of G-protein coupled receptor kinase5 alters agonist-promoted desensitization of β2-adrenergic receptors. *Pharmacogenet. Genomics* **18,** 729–732
13. Liggett, S. B., Cresci, S., Kelly, R. J., Syed, F. M., Matkovich, S. J., Hahn, H. S., Diwan, A., Martini, J. S., Sparks, L., Parekh, R. R., Spertus, J. A., Koch, W. J., Kardia, S. L., and Dorn, G. W., 2nd (2008) A GRK5 polymorphism that inhibits β-adrenergic receptor signaling is protective in heart failure. *Nat. Med.* **14,** 510–517
14. Li, H., Gan, W., Lu, L., Dong, X., Han, X., Hu, C., Yang, Z., Sun, L., Bao, W., Li, P., He, M., Sun, L., Wang, Y., Zhu, J., Ning, Q., *et al.* (2013) A genome-wide association study identifies GRK5 and RASGRP1 as type 2 diabetes loci in Chinese Hans. *Diabetes* **62,** 291–298
15. Kim, J. I., Chakraborty, P., Wang, Z., and Daaka, Y. (2012) G-protein coupled receptor kinase 5 regulates prostate tumor growth. *J. Urol.* **187,** 322–329
16. Chakraborty, P. K., Zhang, Y., Coomes, A. S., Kim, W.-J., Stupay, R., Lynch, L. D., Atkinson, T., Kim, J. I., Nie, Z., and Daaka, Y. (2014) G protein-coupled receptor kinase GRK5 phosphorylates moesin and regulates metastasis in prostate cancer. *Cancer Res.* **74,** 3489–3500
17. Bychkov, E. R., Gurevich, V. V., Joyce, J. N., Benovic, J. L., and Gurevich, E. V. (2008) Arrestins and two receptor kinases are upregulated in Parkinson's disease with dementia. *Neurobiol. Aging* **29,** 379–396
18. Arawaka, S., Wada, M., Goto, S., Karube, H., Sakamoto, M., Ren, C.-H., Koyama, S., Nagasawa, H., Kimura, H., Kawanami, T., Kurita, K., Tajima, K., Daimon, M., Baba, M., Kido, T., *et al.* (2006) The role of G-protein-coupled receptor kinase 5 in pathogenesis of sporadic Parkinson's disease. *J. Neurosci.* **26,** 9227–9238
19. Suo, Z., Cox, A. A., Bartelli, N., Rasul, I., Festoff, B. W., Premont, R. T., and Arendash, G. W. (2007) GRK5 deficiency leads to early Alzheimer-like pathology and working memory impairment. *Neurobiol. Aging* **28,** 1873–1888
20. Chen, Y., Wang, F., Long, H., Chen, Y., Wu, Z., and Ma, L. (2011) GRK5 promotes F-actin bundling and targets bundles to membrane structures to control neuronal morphogenesis. *J. Cell Biol.* **194,** 905–920
21. Sterne-Marr, R., Tesmer, J. J., Day, P. W., Stracquatanio, R. P., Cilente, J.-A., O'Connor, K. E., Pronin, A. N., Benovic, J. L., and Wedegaertner, P. B. (2003) G protein-coupled receptor kinase 2/$G\alpha_{q/11}$ interaction. A novel surface on a regulator of G protein signaling homology domain for binding G α subunits. *J. Biol. Chem.* **278,** 6050–6058
22. Carman, C. V., Barak, L. S., Chen, C., Liu-Chen, L. Y., Onorato, J. J., Kennedy, S. P., Caron, M. G., and Benovic, J. L. (2000) Mutational analysis of Gβγ and phospholipid interaction with G protein-coupled receptor kinase 2. *J. Biol. Chem.* **275,** 10443–10452
23. Pronin, A. N., Satpaev, D. K., Slepak, V. Z., and Benovic, J. L. (1997) Regulation of G protein-coupled receptor kinases by calmodulin and localization of the calmodulin binding domain. *J. Biol. Chem.* **272,** 18273–18280
24. Singh, P., Wang, B., Maeda, T., Palczewski, K., and Tesmer, J. J. (2008) Structures of rhodopsin kinase in different ligand states reveal key elements involved in G protein-coupled receptor kinase activation. *J. Biol. Chem.* **283,** 14053–14062
25. Lodowski, D. T., Barnhill, J. F., Pyskadlo, R. M., Ghirlando, R., Sterne-Marr, R., and Tesmer, J. J. (2005) The role of G βγ and domain interfaces in the activation of G protein-coupled receptor kinase 2. *Biochemistry* **44,** 6958–6970
26. Lodowski, D. T., Pitcher, J. A., Capel, W. D., Lefkowitz, R. J., and Tesmer, J. J. (2003) Keeping G proteins at bay: a complex between G protein-coupled receptor kinase 2 and Gβγ. *Science* **300,** 1256–1262
27. Tesmer, V. M., Kawano, T., Shankaranarayanan, A., Kozasa, T., and Tesmer, J. J. (2005) Snapshot of activated G proteins at the membrane: the

$G\alpha_q$-GRK2-G$\beta\gamma$ complex. *Science* **310,** 1686–1690
28. Lodowski, D. T., Tesmer, V. M., Benovic, J. L., and Tesmer, J. J. (2006) The structure of G protein-coupled receptor kinase (GRK)-6 defines a second lineage of GRKs. *J. Biol. Chem.* **281,** 16785–16793
29. Pao, C. S., Barker, B. L., and Benovic, J. L. (2009) Role of the amino terminus of G protein-coupled receptor kinase 2 in receptor phosphorylation. *Biochemistry* **48,** 7325–7333
30. Boguth, C. A., Singh, P., Huang, C. C., and Tesmer, J. J. (2010) Molecular basis for activation of G protein-coupled receptor kinases. *EMBO J.* **29,** 3249–3259
31. Huang, C.-C., Orban, T., Jastrzebska, B., Palczewski, K., and Tesmer, J. J. (2011) Activation of G protein-coupled receptor kinase 1 involves interactions between its N-terminal region and its kinase domain. *Biochemistry* **50,** 1940–1949
32. Pronin, A. N., Loudon, R. P., and Benovic, J. L. (2002) Characterization of G protein-coupled receptor kinases. *Methods Enzymol.* **343,** 547–559
33. Otwinowski, Z., and Minor, W. (1997) Processing of x-ray diffraction data collected in oscillation mode. *Methods Enzymol.* **276,** 307–326
34. McCoy, A. J. (2007) Solving structures of protein complexes by molecular replacement with Phaser. *Acta Crystallogr. D Biol. Crystallogr.* **63,** 32–41
35. Afonine, P. V., Grosse-Kunstleve, R. W., Echols, N., Headd, J. J., Moriarty, N. W., Mustyakimov, M., Terwilliger, T. C., Urzhumtsev, A., Zwart, P. H., and Adams, P. D. (2012) Towards automated crystallographic structure refinement with phenix.refine. *Acta Crystallogr. D Biol. Crystallogr.* **68,** 352–367
36. Emsley, P., and Cowtan, K. (2004) Coot: model-building tools for molecular graphics. *Acta Crystallogr. D Biol. Crystallogr.* **60,** 2126–2132
37. Chen, V. B., Arendall, W. B., 3rd, Headd, J. J., Keedy, D. A., Immormino, R. M., Kapral, G. J., Murray, L. W., Richardson, J. S., and Richardson, D. C. (2010) MolProbity: All-atom structure validation for macromolecular crystallography. *Acta Crystallogr. D Biol. Crystallogr.* **66,** 12–21
38. Karplus, P. A., and Diederichs, K. (2012) Linking crystallographic model and data quality. *Science* **336,** 1030–1033
39. Krissinel, E., and Henrick, K. (2004) Secondary-structure matching (SSM), a new tool for fast protein structure alignment in three dimensions. *Acta Crystallogr. D Biol. Crystallogr.* **60,** 2256–2268
40. Hayward, S., Kitao, A., and Berendsen, H. J. (1997) Model-free methods of analyzing domain motions in proteins from simulation: a comparison of normal mode analysis and molecular dynamics simulation of lysozyme. *Proteins* **27,** 425–437
41. DeLano, W. L. (2010) *The PyMOL Molecular Graphics System,* Version 1.3r1, Schrödinger, L.LC. New York
42. Dolinsky, T. J., Nielsen, J. E., McCammon, J. A., and Baker, N. A. (2004) PDB2PQR: an automated pipeline for the setup of Poisson-Boltzmann electrostatics calculations. *Nucleic Acids Res.* **32,** W665–W667
43. Adams, P. D., Grosse-Kunstleve, R. W., Hung, L. W., Ioerger, T. R., McCoy, A. J., Moriarty, N. W., Read, R. J., Sacchettini, J. C., Sauter, N. K., and Terwilliger, T. C. (2002) PHENIX: building new software for automated crystallographic structure determination. *Acta Crystallogr. D Biol. Crystallogr.* **58,** 1948–1954
44. Laskowski, R. A., and Swindells, M. B. (2011) LigPlot+: multiple ligand-protein interaction diagrams for drug discovery. *J. Chem. Inf. Model.* **51,** 2778–2786
45. Laue, T. M., Shah, B. D., Ridgeway, T. M., and Pelletier, S. L. (1992) in *Analytical Ultracentrifugation in Biochemistry and Polymer Science* (Harding, S. E., Rowe, A. J., and Horton, J. C., eds) pp. 90–125, Royal Society of Chemistry, Cambridge, UK
46. Schuck, P. (2000) Size-distribution analysis of macromolecules by sedimentation velocity ultracentrifugation and lamm equation modeling. *Biophys. J.* **78,** 1606–1619
47. Loomis, C. R., and Bell, R. M. (1988) Sangivamycin, a nucleoside analogue, is a potent inhibitor of protein kinase C. *J. Biol. Chem.* **263,** 1682–1692
48. Tesmer, J. J. (2009) Structure and function of regulator of G protein signaling homology domains. *Prog. Mol. Biol. Transl. Sci.* **86,** 75–113
49. Pronin, A. N., Carman, C. V., and Benovic, J. L. (1998) Structure-function analysis of G protein-coupled receptor kinase-5. Role of the carboxyl terminus in kinase regulation. *J. Biol. Chem.* **273,** 31510–31518
50. Thiyagarajan, M. M., Stracquatanio, R. P., Pronin, A. N., Evanko, D. S., Benovic, J. L., and Wedegaertner, P. B. (2004) A predicted amphipathic helix mediates plasma membrane localization of GRK5. *J. Biol. Chem.* **279,** 17989–17995
51. Pitcher, J. A., Fredericks, Z. L., Stone, W. C., Premont, R. T., Stoffel, R. H., Koch, W. J., and Lefkowitz, R. J. (1996) Phosphatidylinositol 4,5-bisphosphate (PIP_2)-enhanced G protein-coupled receptor kinase (GRK) activity. Location, structure, and regulation of the PIP2 binding site distinguishes the GRK subfamilies. *J. Biol. Chem.* **271,** 24907–24913
52. Tesmer, J. J., Nance, M. R., Singh, P., and Lee, H. (2012) Structure of a monomeric variant of rhodopsin kinase at 2.5 Å resolution. *Acta Crystallogr. Sect. F Struct. Biol. Cryst. Commun.* **68,** 622–625
53. Xu, H., Jiang, X., Shen, K., Fischer, C. C., and Wedegaertner, P. B. (2014) The regulator of G protein signaling (RGS) domain of G protein-coupled receptor kinase 5 (GRK5) regulates plasma membrane localization and function. *Mol. Biol. Cell* **25,** 2105–2115
54. Taylor, S. S., Yang, J., Wu, J., Haste, N. M., Radzio-Andzelm, E., and Anand, G. (2004) PKA: a portrait of protein kinase dynamics. *Biochim. Biophys. Acta* **1697,** 259–269
55. Zhang, P., Smith-Nguyen, E. V., Keshwani, M. M., Deal, M. S., Kornev, A. P., and Taylor, S. S. (2012) Structure and allostery of the PKA RIIβ tetrameric holoenzyme. *Science* **335,** 712–716
56. Yang, J., Ten Eyck, L. F., Xuong, N. H., and Taylor, S. S. (2004) Crystal structure of a cAMP-dependent protein kinase mutant at 1.26 Å: new insights into the catalytic mechanism. *J. Mol. Biol.* **336,** 4734–4787
57. Bastidas, A. C., Deal, M. S., Steichen, J. M., Keshwani, M. M., Guo, Y., and Taylor, S. S. (2012) Role of N-terminal myristylation in the structure and regulation of cAMP-dependent protein kinase. *J. Mol. Biol.* **422,** 215–229
58. Yang, J., Cron, P., Good, V. M., Thompson, V., Hemmings, B. A., and Barford, D. (2002) Crystal structure of an activated Akt/protein kinase B ternary complex with GSK3-peptide and AMP-PNP. *Nat. Struct. Biol.* **9,** 940–944
59. Shaltiel, S., Cox, S., and Taylor, S. S. (1998) Conserved water molecules contribute to the extensive network of interactions at the active site of protein kinase A. *Proc. Natl. Acad. Sci. U.S.A.* **95,** 484–491
60. Huse, M., and Kuriyan, J. (2002) The conformational plasticity of protein kinases. *Cell* **109,** 275–282
61. Hemmer, W., McGlone, M., Tsigelny, I., and Taylor, S. S. (1997) Role of the glycine triad in the ATP-binding site of cAMP-dependent protein kinase. *J. Biol. Chem.* **272,** 16946–16954
62. Akamine, P., Madhusudan, Wu, J., Xuong, N.-H., Ten Eyck, L. F., and Taylor, S. S. (2003) Dynamic features of cAMP-dependent protein kinase revealed by apoenzyme crystal structure. *J. Mol. Biol.* **327,** 159–171
63. Kannan, N., Haste, N., Taylor, S. S., and Neuwald, A. F. (2007) The hallmark of AGC kinase functional divergence is its C-terminal tail, a cis-acting regulatory module. *Proc. Natl. Acad. Sci. U.S.A.* **104,** 1272–1277
64. Narayana, N., Cox, S., Nguyen-huu, X., Ten Eyck, L. F., and Taylor, S. S. (1997) A binary complex of the catalytic subunit of cAMP-dependent protein kinase and adenosine further defines conformational flexibility. *Structure* **5,** 921–935
65. Yang, J., Kennedy, E. J., Wu, J., Deal, M. S., Pennypacker, J., Ghosh, G., and Taylor, S. S. (2009) Contribution of noncatalytic core residues to activity and regulation in protein kinase A. *J. Biol. Chem.* **284,** 6241–6248
66. Batkin, M., Schvartz, I., and Shaltiel, S. (2000) Snapping of the carboxyl terminal tail of the catalytic subunit of PKA onto its core: characterization of the sites by mutagenesis. *Biochemistry* **39,** 5366–5373
67. Zhou, J., and Adams, J. A. (1997) Participation of ADP dissociation in the rate-determining step in cAMP-dependent protein kinase. *Biochemistry* **36,** 15733–15738
68. Bastidas, A. C., Wu, J., and Taylor, S. S. (2015) Molecular features of product release for the PKA catalytic cycle. *Biochemistry* **54,** 2–10
69. Thal, D. M., Homan, K. T., Chen, J., Wu, E. K., Hinkle, P. M., Huang, Z. M., Chuprun, J. K., Song, J., Gao, E., Cheung, J. Y., Sklar, L. A., Koch, W. J., and Tesmer, J. J. (2012) Paroxetine is a direct inhibitor of G protein-coupled receptor kinase 2 and increases myocardial contractility. *ACS Chem. Biol.* **7,** 1830–1839
70. Kunapuli, P., Gurevich, V. V., and Benovic, J. L. (1994) Phospholipid-stimulated autophosphorylation activates the G protein-coupled receptor

kinase GRK5. *J. Biol. Chem.* **269,** 11209–11212
71. Buczyłko, J., Gutmann, C., and Palczewski, K. (1991) Regulation of rhodopsin kinase by autophosphorylation. *Proc. Natl. Acad. Sci. U.S.A.* **88,** 2568–2572
72. Levay, K., Satpaev, D. K., Pronin, A. N., Benovic, J. L., and Slepak, V. Z. (1998) Localization of the sites for Ca^{2+}-binding proteins on G protein-coupled receptor kinases. *Biochemistry* **37,** 13650–13659
73. Tidow, H., and Nissen, P. (2013) Structural diversity of calmodulin binding to its target sites. *FEBS J.* **280,** 5551–5565
74. O'Neil, K. T., and DeGrado, W. F. (1990) How calmodulin binds its targets: sequence independent recognition of amphiphilic α-helices. *Trends Biochem. Sci.* **15,** 59–64
75. Blundell, T. L., and Johnson, L. N. (1976) *Protein Crystallography*, pp. 375–377, Academic Press, London
76. Arndt, U. W., Crowther, R. A., and Mallett, J. F. (1968) A computer-linked cathode-ray tube microdensitometer for x-ray crystallography. *J. Sci. Instrum.* **1,** 510–516
77. Diederichs, K., and Karplus, P. A. (1997) Improved R-factors for diffraction data analysis in macromolecular crystallography. *Nat. Struct. Biol.* **4,** 269–275
78. Weiss, M. S. (2001) Global indicators of X-ray data quality. *J. Appl. Crystallogr.* **34,** 130–135
79. Brünger, A. T. (1992) Free R value: a novel statistical quantity for assessing the accuracy of crystal structures. *Nature* **355,** 472–475
80. Krissinel, E., and Henrick, K. (2007) Inference of macromolecular assemblies from crystalline state. *J. Mol. Biol.* **372,** 774–797
81. Homan, K. T., Waldschmidt, H. V., Glukhova, A., Cannavo, A., Song, J., Cheung, J. Y., Koch, W. J., Larsen, S. D., and Tesmer, J, J. (2015) Crystal structure of G protein-coupled receptor kinase 5 in complex with a rationally designed inhibitor. *J. Biol. Chem.* **290,** M115.647370

Atomic Structure of GRK5 Reveals Distinct Structural Features Novel for G Protein-coupled Receptor Kinases

Konstantin E. Komolov, Anshul Bhardwaj and Jeffrey L. Benovic

J. Biol. Chem. 2015, 290:20629-20647.
doi: 10.1074/jbc.M115.647297 originally published online June 1, 2015